Volume 6

LLE Review

Quarterly Report

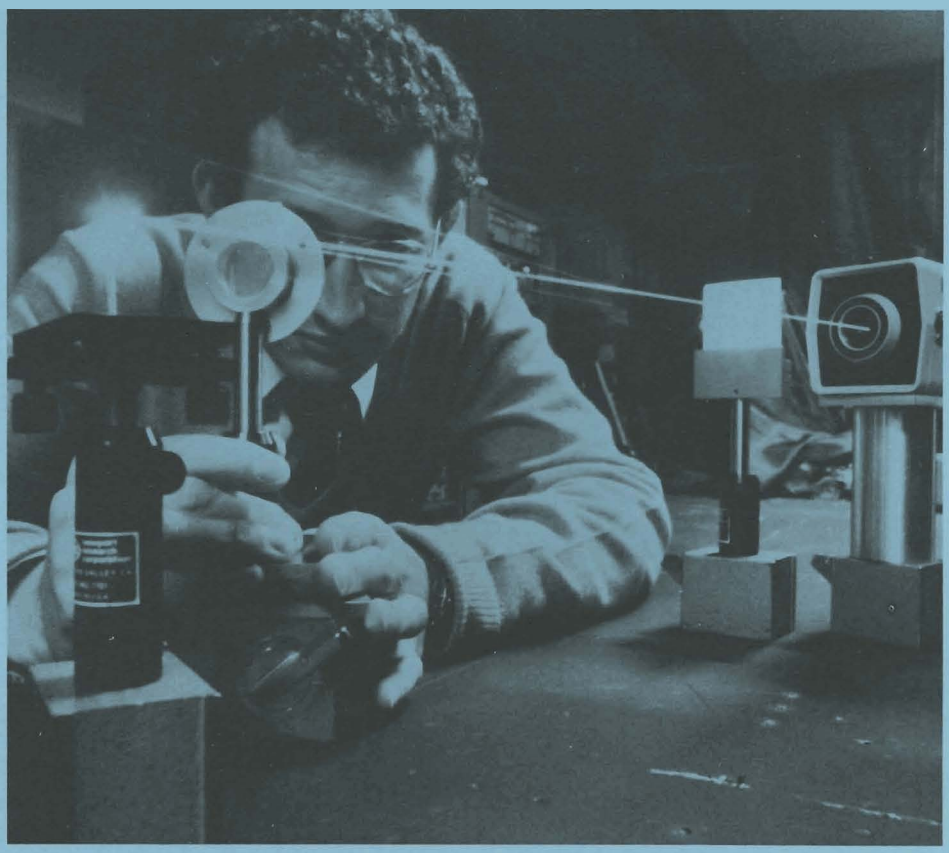

January, 1981 — March, 1981

Laboratory for Laser Energetics
College of Engineering and Applied Science
University of Rochester
250 East River Road
Rochester, New York 14623

Volume 6

LLE Review

Quarterly Report

Editor: John A. Boles
(716-275-2315)

January, 1981 — March, 1981

Laboratory for Laser Energetics
College of Engineering and Applied Science
University of Rochester
250 East River Road
Rochester, New York 14623

IN BRIEF

Experiments to measure the interaction of ultraviolet light with several different target materials continue to produce significant new research results. Most notable was the measurement of x-rays produced by the targets. Incident laser energy was converted to x-ray lines with efficiencies of 1% at 1.8 KeV (Si lines). Nickel x-ray lines at 7.8 KeV were produced with 0.1% efficiency.

In addition, highlights of other recent developments include:

- Liquid crystals may be utilized to design large aperture waveplates.
- Simple modification of the LLE 600 psec oscillator produced an oscillator capable of generating 1.15 nsec pulses with ± 4% stability.
- Active and passive stabilization of the synchronously pumped dye laser reported in LLE Review, Volume 5 reduced the sources of instability and produced pulses shorter than 300 fsec.
- Modeling of the interaction of intense electromagnetic waves with a plasma has determined the threshold and growth rate for a filamentation instability. These narrow filaments of high intensity and low plasma density will form at laser intensities above 10^{14} W/cm^2.

CONTENTS

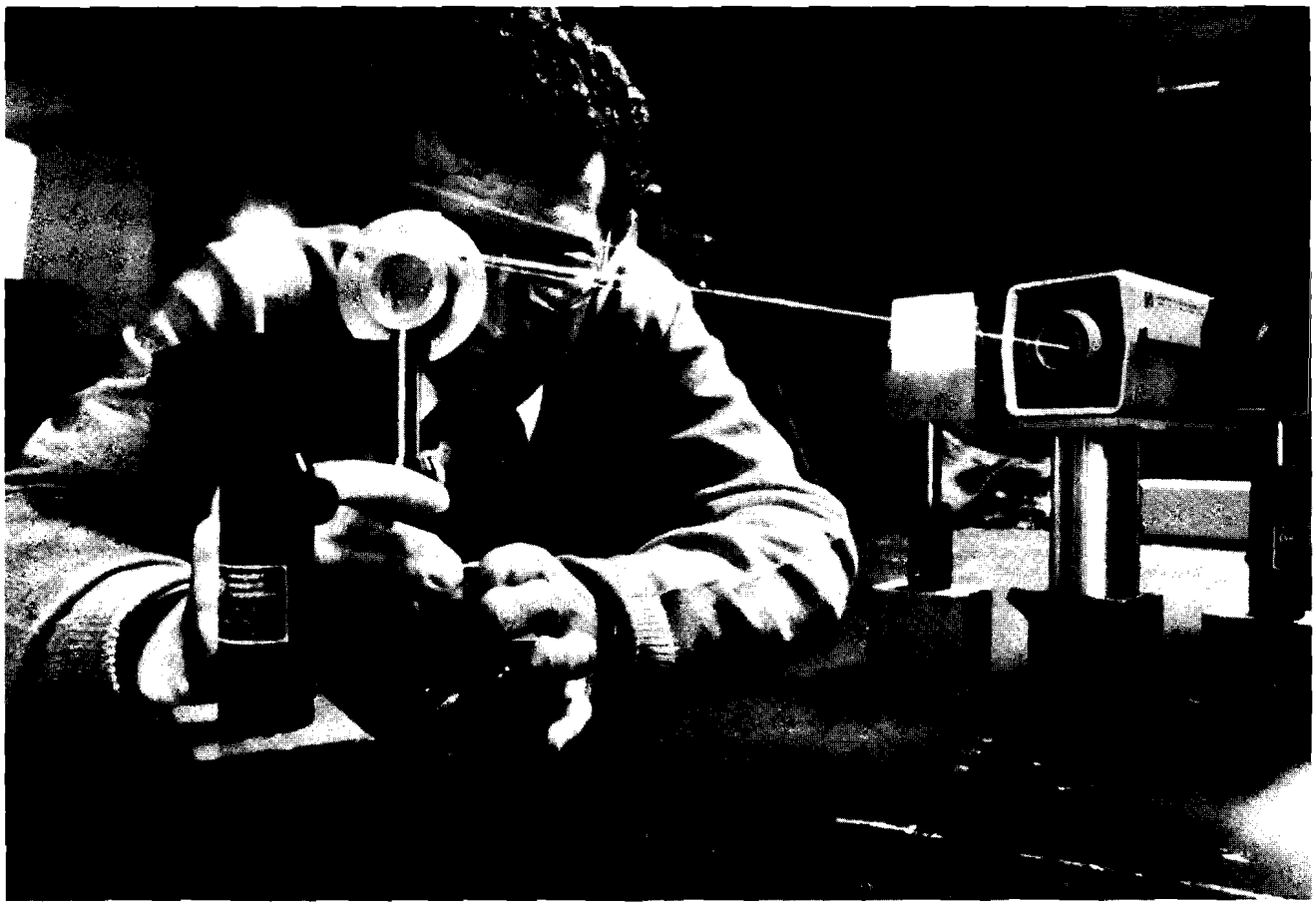

Steve Jacobs testing performance of liquid crystal isolator. These passive devices hold promise as large scale isolators for high power laser systems. This review reports on the design of liquid crystal waveplates and their potential for replacing more expensive optical materials.

Section 1
LASER SYSTEM REPORT

1.A OMEGA Facility Report

Tests to evaluate the spatial intensity distribution of an OMEGA beam at the location of a target were conducted this quarter. In addition, the 24 beam laser was prepared for the first series of target experiments scheduled for later in the year.

The near field photographs discussed in Volume 5 of the LLE Review were digitized and processed on the LLE Cyber 175. Extensive cross checks of the calibration of this process were performed. It is anticipated that these photographs will provide the data to normalize several beam propagation codes during the following quarter.

A series of shots were taken on OMEGA to study the optical properties of the laser beam at the end of the laser and at the target chamber focus lens. Near field cameras were used at both locations to measure the pulsed beam intensity distribution and shearing interferometry was used at both locations to measure the pulsed beam phase distribution. In addition, far field array cameras recorded the intensity distribution from best focus to approximately 1,200 μm inside of focus on the OMEGA focus lens. This data is now being reduced to compare to calculations and to provide a baseline characterization of a typical OMEGA beamline at 100 psec and at 600 psec.

1.B Liquid Crystal Devices for High Powered Lasers – Part 2: Waveplates

The ability to manipulate the state of polarization of laser radiation is fundamental to successful operation of large laser systems like LLE's OMEGA. Propagation of circularly polarized light through large rod amplifiers maximizes system output power.[1] Electro-optic switching of linearly polarized light with Pockels cells[2] suppresses amplified spontaneous emission (ASE)[3] and provides isolation between amplification stages. Rotation of the plane of polarization for linearly polarized light incident on beamsplitting mirrors determines beam energy balance among the arms of multiple beam systems. This control over the polarization state of light in a laser system is achieved through the use of passive optical devices called phase retardation plates, or waveplates. Although traditionally fabricated from optically birefringent *solid* single crystal materials like quartz or mica, waveplates can be made from a class of *liquid* crystals called nematics. This article discusses the physical properties of nematic liquid crystals, their relationship to optical birefringence, and the potential advantages offered by nematic liquid crystal waveplates.

Of the various types of liquid crystals (cholesterics were discussed in Volume 5 of the LLE Review) nematic compounds have made the largest impact in the marketplace. Information displays using

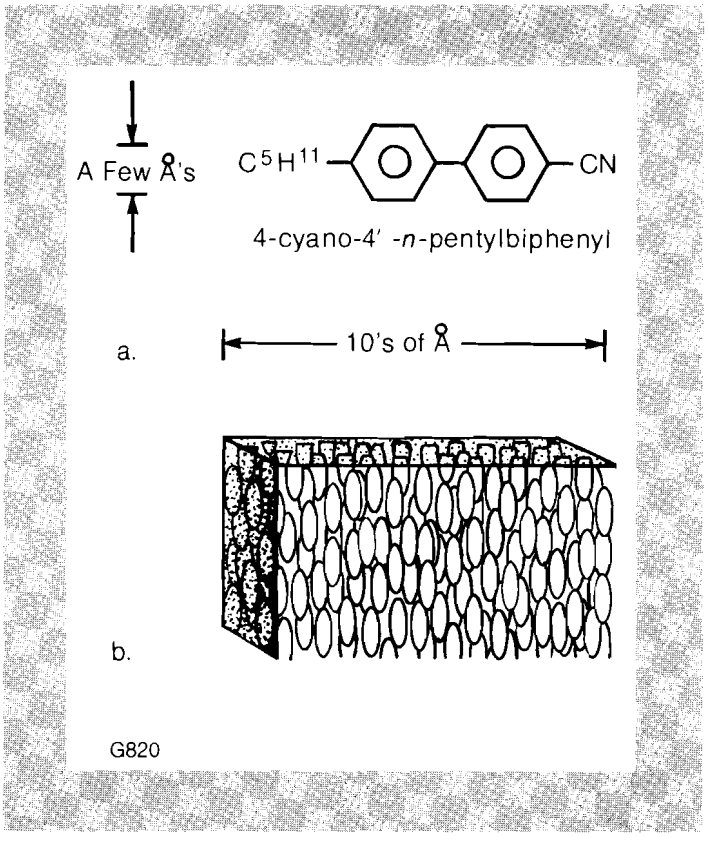

Fig. 1a
Structure of nematic liquid crystal. A nematic liquid crystal molecule consists of carbon/hydrogen bonds connected by benzene rings. The properties of this compound, K15, are given in the text.

Fig. 1b
Alignment of liquid crystal molecules. In the nematic phase, all liquid crystal molecules align spontaneously through the bulk with their longitudinal axes parallel.

nematics are commonly found in digital watches, calculators, and electronic games.[4] This commercial success is due to the unique physical properties of the nematic liquid crystal phase. Nematics possess the structure depicted in Fig. 1a, wherein chains of hydrocarbons are connected by benzene rings to form long, rigid, rodlike molecules. The most striking feature of nematics in bulk form is the tendency of these rodlike molecules to spontaneously align with their long axes parallel throughout their volume, as in Fig. 1b. The spatial order so obtained imparts crystalline behavior to the nematic, simultaneously preserving its fluid-like properties of low viscosity and flow. The composition and shape of nematic molecules and their preference for spontaneous alignment form the basis for their unique optical properties.

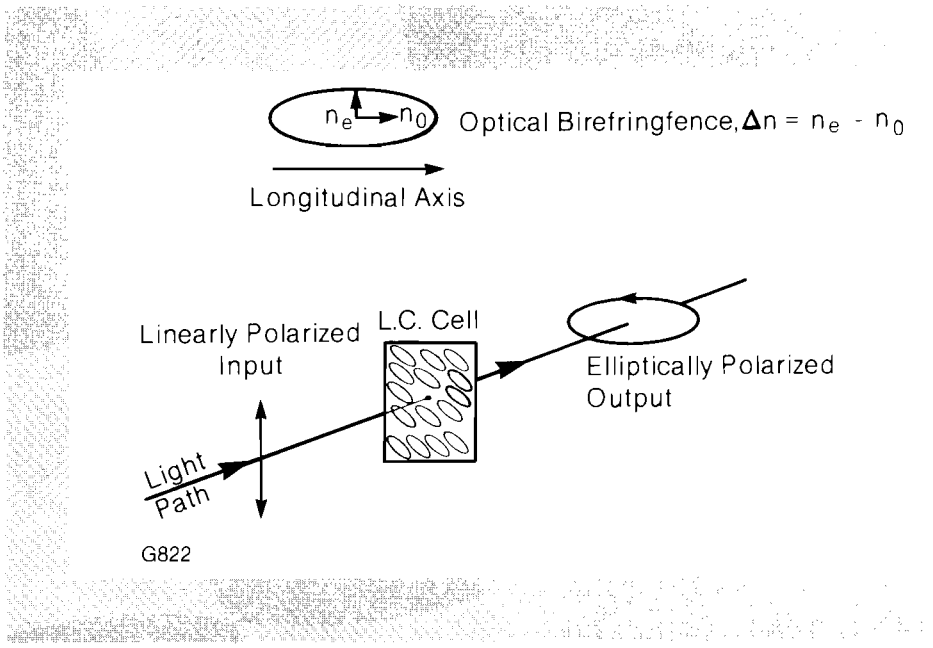

Fig. 2
Propagation of polarized light through nematic liquid crystal. Nematic liquid crystals exhibit a refractive index that depends upon the propagation direction and polarization vibration direction of incident light. Orthogonal components of linearly polarized light that enter a nematic vibrating in phase will emerge with one component's phase retarded with respect to the other. The emerging light will in general be elliptically polarized.

Nematic molecules are optically birefringent. Light incident upon a layer of oriented nematic fluid will propagate through it with a speed that depends upon whether the light polarization vibration direction is parallel or perpendicular to the long axes of the nematic molecules. As shown in Fig. 2, a nematic molecule resembles a uniaxial crystal in that it has two different refractive indices, n_o and n_e. Birefringence is defined as the difference between these two values, $\Delta n = n_e - n_o$. In nematics n_o may be larger or smaller than n_e. If it is larger, then light propagating through the liquid layer with a polarization vibration direction parallel to the long axes of the molecules travels more slowly than its orthogonal component. If the two components were in phase upon entering the liquid layer, they will be out of phase after leaving the liquid by an amount given by:

$$\delta = \frac{2\pi}{\lambda} t\Delta n$$

where δ is the amount of phase retardation, λ is the wavelength of optical radiation, and t is the thickness of birefringent material

traversed. This phase retardation is the key to the use of liquid crystals as waveplates.

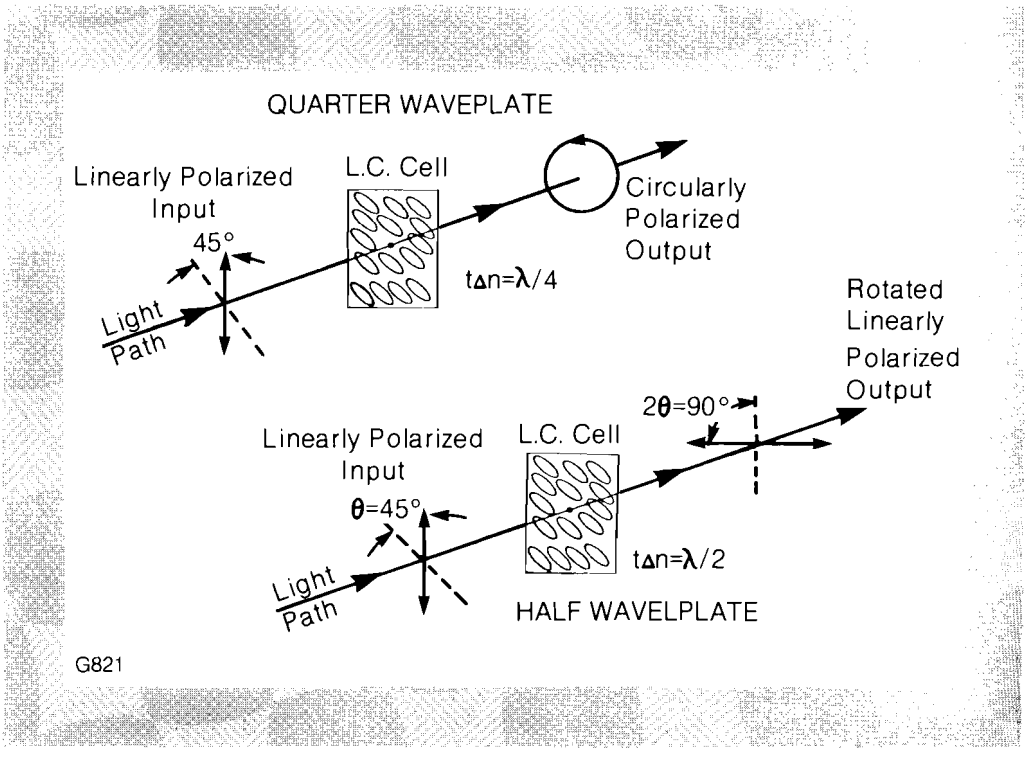

Fig. 3
Quarter waveplate and half waveplate conditions. In the special case where nematic liquid crystal thickness (t) times birefringence (Δn) equals a quarter wavelength, incident linearly polarized light will emerge circularly polarized. Incident linearly polarized light will emerge with its plane of polarization rotated by an angle 2θ when tΔn equals one half wavelength.

Two types of waveplates are required for the polarization manipulations described at the beginning of this article. Quarter waveplates convert linearly to circularly polarized light by introducing a 90 degree phase shift (δ=90°) to optical radiation, and half waveplates rotate the plane of vibration of linearly polarized light by introducing a 180 degree phase shift (δ=180°) (see Fig. 3). Table 1 gives the birefringence, and thickness required to fabricate half waveplates from nematics compared to quartz and mica at $\lambda = 1.05\ \mu$m.

It is clear from Table 1 that nematics are order of magnitude more birefringent than solid crystalline materials. It is therefore necessary to produce liquid crystals in thin layers to achieve appropriate values of retardance.

Material:	Mica	Quartz	Nematics
Δn:	0.003	0.0088	0.08 - 0.25
t (λ/2),μm:	175	60	6 - 2

G814

Table 1
Optical properties of nematics compared to quartz and mica for half waveplate applications at $\lambda = 1.05\mu$.

The components of nematic liquid crystal waveplates are shown in Fig. 4. Prior to assembling a cell as a liquid crystal sandwich with mylar spacers, the inner cell substrate surfaces must be rubbed unindirectionally with quarter micron diamond paste. This commonly prescribed technique[5] forces the nematic molecules into alignment with their long axes parallel to the surfaces of the substrates. Thus anchored at each wall, the bulk of the nematic fluid spontaneously aligns as depicted in Fig. 4. With its rub direction oriented at 45° to the polarization direction of incident optical radiation, the cell functions as a waveplate, with capabilities not easily achieved with solid crystals.

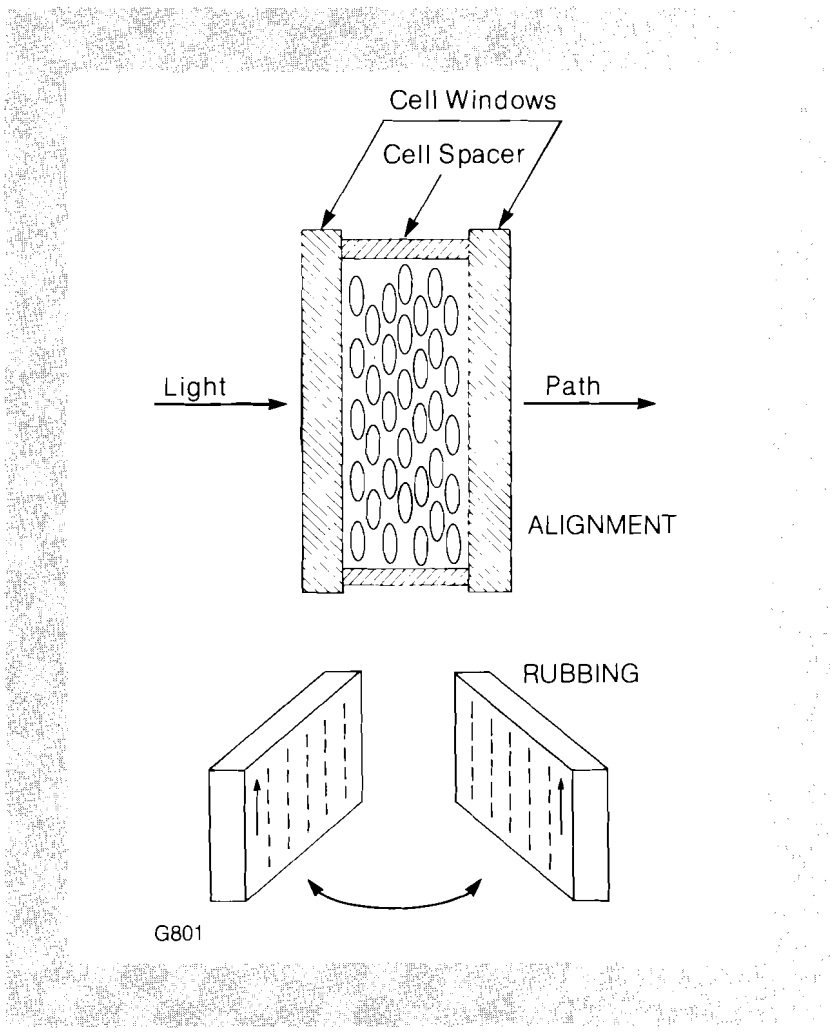

Fig. 4
Substrate support required for thin liquid crystal waveplates. A sandwich is made with the nematic fluid layer filling a gap between two glass plates whose separation is fixed with mylar spacers 1 - 10 μm thick. Molecular alignment parallel to the substrate surfaces is assured by unidirectionally rubbing the glass plates with diamond paste prior to assembly.

The primary advantage of nematic liquid crystals as waveplates is the ability to fabricate them in large sizes. Mica is very difficult to obtain in apertures larger than 1500 mm, and the avilability of large stones of natural single crystal quartz with adequate optical quality has greatly diminished in the past 5 years. The useful aperture of a liquid crystal waveplate, however, is limited only by the dimensions of the glass substrates that comprise the cell. There is a problem in constructing cells whose liquid layer thickness is maintained at a constant value across the device

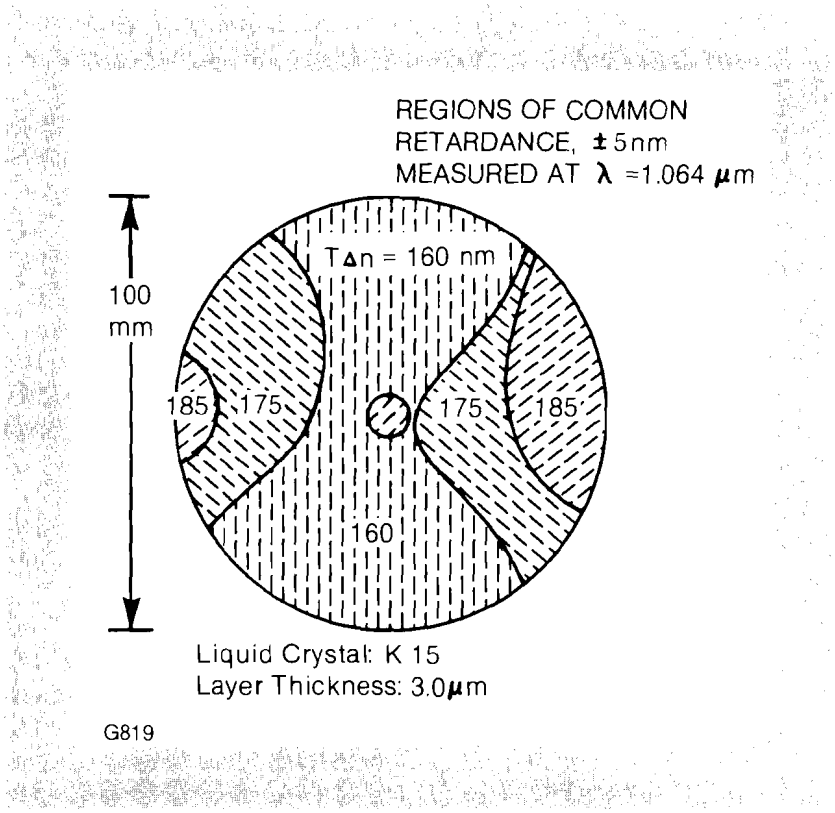

Fig. 5
Retardance contour plot of a 100 mm diameter liquid crystal waveplate. The problem of uniform retardance can be solved by the use of thicker windows. The BK-7 windows which comprise this cell were 9 mm thick.

aperture. Figure 5 gives a contour plot measured on a 100 mm diameter liquid crystal cell whose glass substrates were not thick enough to support a uniform gap thickness of 6 μm. Cell windows with a lower aspect ratio and perhaps the use of nematics with a somewhat smaller birefringence (see Table 2) should enable larger devices with uniform retardance profiles to be constructed.

Vendor:		Merck	Hoffman LaRoche	BDH
Material:		ZLI-1646	TN-2080	K15
Viscosity, cst:		26	36	--
Temp. Range, °C:		-7 to +60	-5 to +72	24 to 35
Birefringence:	n_e	1.565	1.610	1.702
@λ=0.589μm	n_0	1.480	1.489	1.539
	Δn	0.085	0.121	0.163

G815

Table 2
Properties of 3 commercial nematics used in the fabrication of waveplates at LLE. Note the birefringence ranges available and the temperature regions over which useful operations may be expected.

A second advantage to liquid crystals is the flexibility of design they offer in waveplate applications. Because of their large birefringence, thin liquid crystal layers provide the retardation required in most waveplate applications. This makes them less sensitive to the angle of incidence of incoming radiation than solids (see Fig. 6). A large acceptance angle relaxes alignment requirements in laser system applications.

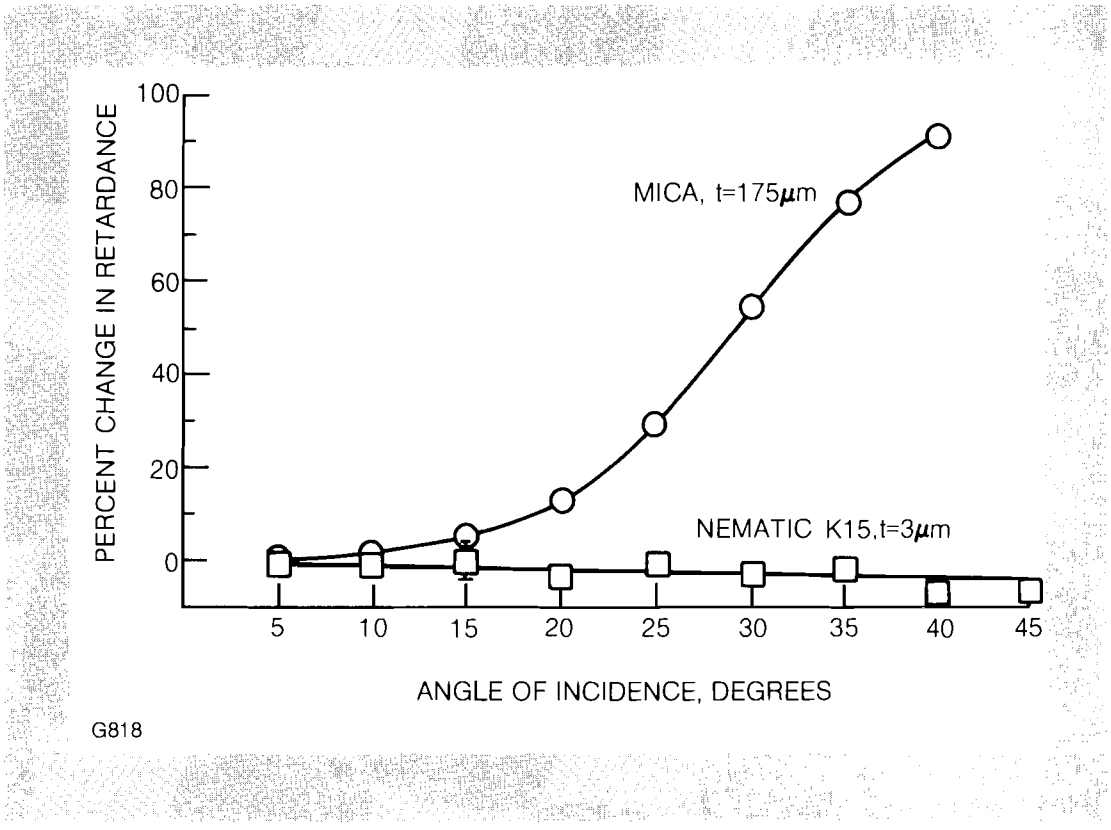

Fig. 6
Retardance versus angle of incidence. Liquid crystal waveplates exhibit minimal angular sensitivity when compared to solid crystal alternatives. Measurements made with a 1 mm diameter CW:Yag laser show the nematic K15 to be insensitive to angle of incidence when compared to mica.

This design flexibility is also evident in the application of liquid crystals as radially birefringent waveplates. Figure 7 shows how, by putting a few waves of curvature on the inner surface of a glass flat, one can then assemble a cell whose liquid thickness (and therefore cell retardance) decreases radially from center to edge. Weak birefringent lenses composed of crystal quartz have recently been proposed as a means for constructing soft apertures for lasers.[6] By index matching to the substrate, a liquid crystal radially birefringent element would remove the requirement for a correcting lens in such a scheme.

This article has explained how the nematic class of liquid crystal compounds might be used to fabricate waveplates for large aperture laser systems. Some of the advantages to the use of liquid crystals in place of solid crystals have been discussed. Preliminary measurements have shown that, although more work is required, liquid crystals can be aligned over large areas and oriented to operate as waveplates. The laser damage threshold of liquid crystals and their potential for use at other wavelengths will be the subject of future research.

REFERENCES

1. W. Seka, J. Soures. O. Lewis, J. Bunkenburg, D. Brown, S. Jacobs, G. Mourou, and J. Zimmerman, *Appl. Opt.* **19** 409-419 (1980).
2. L. L. Steinmetz, T. W. Pouliot, and B. C. Johnson, *Appl. Opt.* **12** 1468-1471 (1973).

3. G. Mourou, J. Bunkenburg, and W. Seka *Optics Communications* **34** 252-254 (1980).
4. See, for example *The Physics and Chemistry of Liquid Crystal Devices,* Ed. by Gerald J. Sprockel, Plenum Press, New York, 1980.
5. G. Meir, E. Sackman, and J. G. Grabmaier, *Applications of Liquid Crystals* **99,** Springer Verlag, New York, 1975.
6. G. Giuliani, Y. K. Park, and R. L. Byer, *Optics Letters* **5** 491-493 (1980).

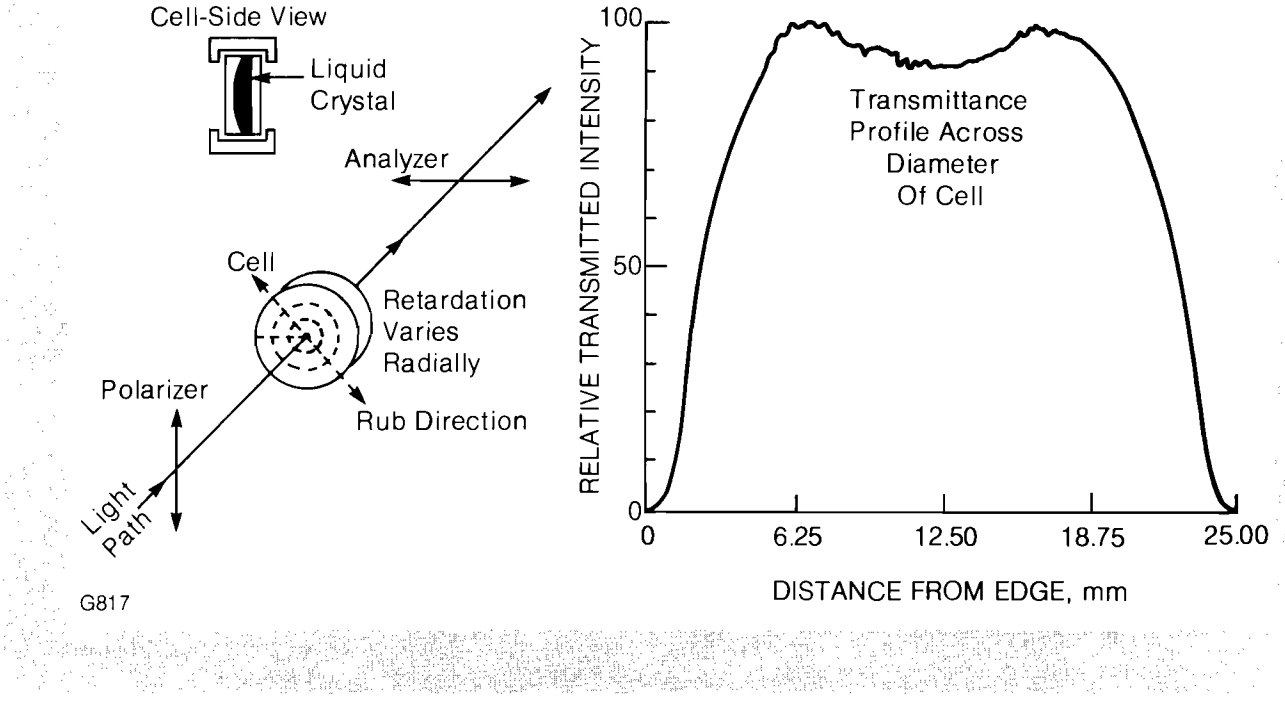

Fig. 7
Fabrication of waveplates with radially varying retardance. Liquid crystals may be used to construct waveplates with radially varying retardance. Filling the air gap between a weak lens and a flat, a liquid crystal radially birefringent element could serve in conjunction with a polarizer as a soft aperture. The transmittance profile for a 25 mm diameter cell oriented between crossed polarizers and scanned across its diameter using a 1 mm CW:Yag laser beam, shows that an internal sag of 8 μm is adequate to give just over one half wave of retardation at cell center using nematic TN-2080.

1.C Active-Passive Mode-Locked Oscillator Generating Nanosecond Pulses

Laser oscillators operating at 1.054 μm are needed to drive phosphate-based glass laser amplifier chains optimally. For explosive pusher mode laser fusion experiments, one of the important parameters is peak power. Consequently, short pulse oscillators have been designed which operate reliably between 50 psec and 600 psec FWHM pulse duration.[1] Recent advances towards ablative or quasi-ablative target compressions[2] and high efficiency frequency conversions[3] have made reliable optical oscillators generating pulses between 1 nsec and 1.2 nsec duration necessary. Actively mode-locked oscillators fulfill this requirement; they offer high repetition rates, quick tuning of the pulse duration, and very good pulse duration and amplitude stability.[4] Their disadvantage, however, is high cost largely due to

a complicated electronic package compared to an LC-discharge network driving a conventional oscillator. Operating a passive oscillator in the monomode regime[5] is also possible, but the reproducibility and absence of substructures in the pulse are often not considered sufficient for target irradiation experiments. Regenerative amplifier[6,7] systems are able to produce injection-locked pulses which can be stretched up to 1.5 nsec FWHM; at that duration, however, their amplitude stability is not yet truly satisfactory.

The Laboratory for Laser Energetics has developed an active-passive mode-locked oscillator with much the same characteristics of earlier oscillators,[1] which is capable of generating optical pulses of up to 1.4 nsec duration.

Presently, the oscillator described in Ref. 1 is used in the University of Rochester's laser systems GDL[8] and OMEGA.[9] Though very reliable as a short pulse oscillator, pulses longer than 700 psec cannot be achieved with the required stability and absence of substructures. The reason for this limit can be understood as follows:

- For a cavity length of 1.5 m and a gain bandwidth of 20 nm, the laser runs on about 2.5×10^4 longitudinal modes when pumped 20% above threshold.

- An etalon with a finesse of 2 and an optical thickness of 5.88 mm restricts the FWHM bandwidth to approximately 0.048 nm so that the laser will run on about 65 modes. With such a laser we observe still reproducible pulses of $<$700 psec duration. If the number of modes drops much below the above value however, one finds incomplete mode-locking, poor stability, satellite pulses, and occasional no lases.

In order to further restrict the lasing bandwidth without restricting the number of modes on which the laser is running, the cavity length has to be increased. Therefore, doubling the cavity length limits the bandpass by a factor of two (e.g., an etalon with finesse = 2, thickness = 8, index = 1.47) while maintaining the number of modes and hence the major stability characteristics of the oscillator.

Apart from the thickest etalon as a bandwidth-restricting element, the laser contains two bandwidth-generating elements, namely the dye and the AO (acousto-optic) modulator. The pulse duration τ_{AO}, resulting from etalon and AO modulator only, can be calculated quite well using the theory for active mode-locking described in Ref. 10. Differences between theory and experiment arise from a lack of buildup time to ensure Fourier transform-limited mode-locking.[11,12] The pulse duration τ_D resulting from etalon and dye only is much harder to calculate as the process of the transient mode-locking of a gradually bleaching dye is very complex and we are not aware of a closed form solution to this problem. The contribution of dye and etalon to the pulse duration, however,

can easily be measured. The final pulse duration due to both processes can, assuming Gaussian pulses in each case be obtained via:

$$\frac{1}{\tau^2} = \frac{1}{\tau_{AO}^2} + \frac{1}{\tau_D^2}$$

Our 1.5 m oscillator as well as our 3 m oscillator when Q-switched with a slow dye follow this relationship closely.

The experimental layout is shown in Fig. 8. To keep the laser cavity within manageable dimensions, we used two dielectric mirrors (R_{max} at 45°) to fold the cavity.

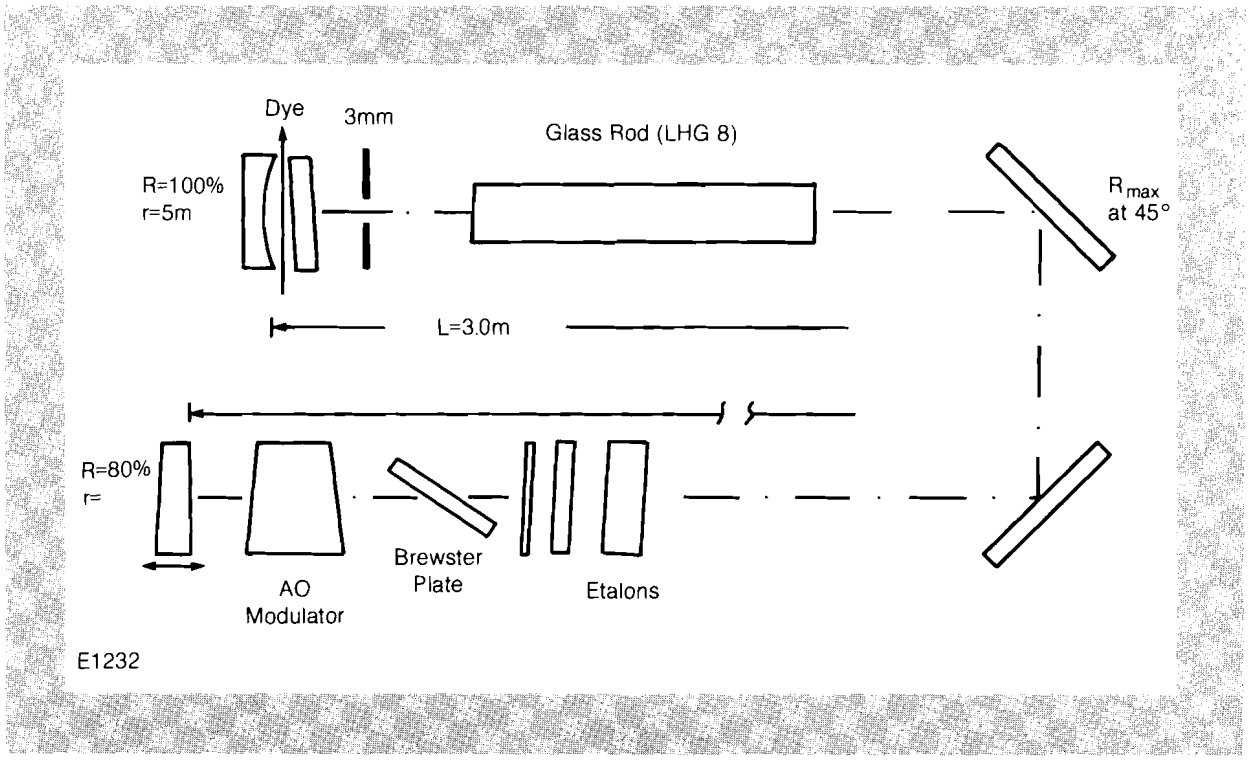

Fig. 8
Schematic layout of the oscillator cavity. An oscillator capable of generating optical pulses up to 1.4 nsec was built with only small modification of a 600 psec oscillator.

The pump cavity was a double elliptical unit (Raytheon LC-73) which uses two FX6-81-C4 flashlamps in series. A pulse forming network was used to form a current pulse of about 240 μsec duration discharged through the flashlamps. This current pulse makes it possible to increase the fluorescence power from the laser rod more gradually, such that the nonlinear bleaching phase of the dye becomes as long as possible. This ensures a maximum number of passes through the AO modulator, hence the closest approach to complete mode-locking during the lasing-buildup phase.[11,12]

The laser was Q-switched with a slow Ni dye (Eastman Kodak Ni dye #14015) such that the contribution of the dye to the shortening of individual pulses was less than that of the modulator. Accordingly, the modulator dominates the observed pulse duration.

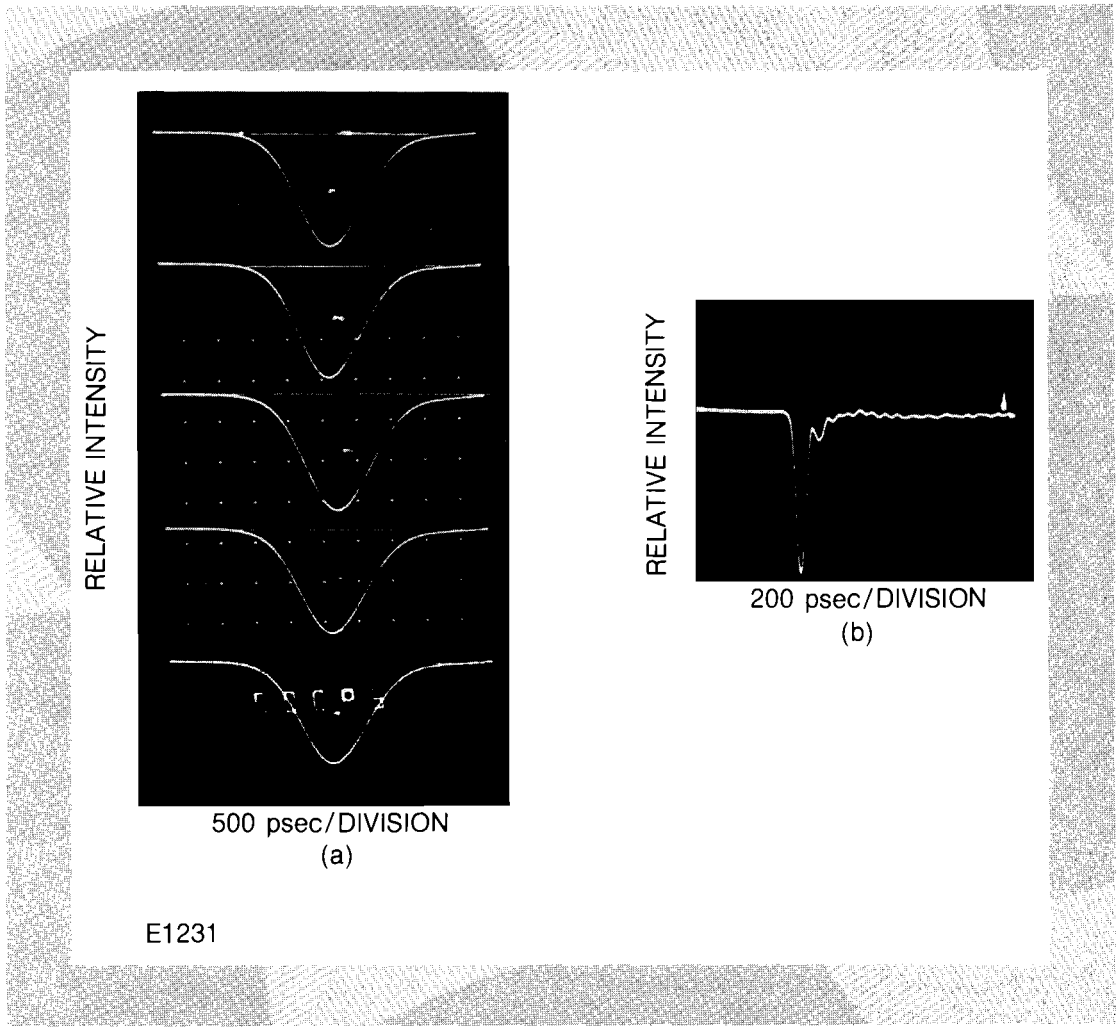

Fig. 9a
Laser output pulses. Shown are five consecutive shots. The oscillator exhibits amplitude stability of ± 4%.

Fig. 9b
Response time of the detector and scope.

Figure 9a shows a sequence of five consecutive shots, the response of the detection system is shown in Fig. 9b. The pulse duration is 1.15 ± 0.06 nsec, the relative amplitude stability of the envelope of the output train was measured to be ± 4%, with single pulse energies up to 0.6 mJ. Figure 10 shows a streak of the frequency-doubled pulse which verifies the absence of sub-structures in the red pulse to within 2% amplitude modulation.

Only relatively small modifications to a 1.5 m cavity[1] are needed to achieve these results. From the theoretical considerations, it can be expected that the limit of the system is a pulse of 1.4 nsec duration, obtainable with BK7 etalons of finesse 2 and 8 mm thickness. The separation between pulses of 20 nsec provides for easy single pulse switch out. This oscillator represents a useful addition to the possibilities of generating a stable mode-locked laser pulse in the nanosecond regime.

REFERENCES

1. W. Seka, J. Bunkenburg, *J. Appl. Phys.* **49,** 2277 (1978).

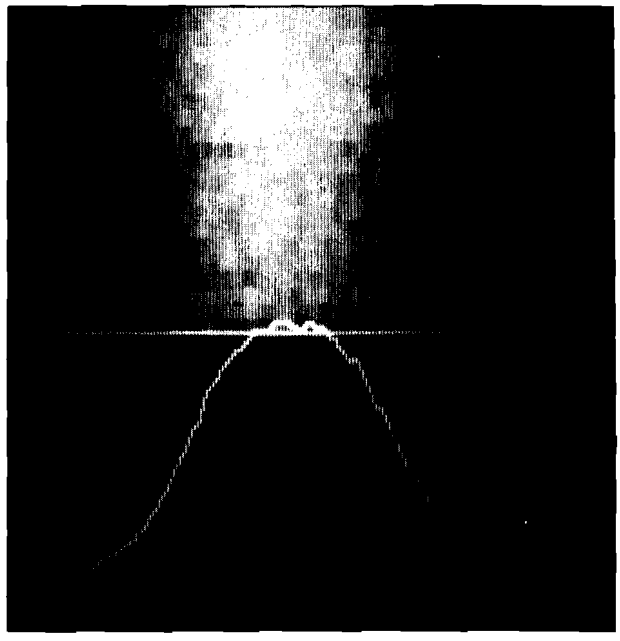

Fig. 10
Streak record of the frequency doubled single 1.15 nsec pulse. Streaks of the frequency doubled pulse verify the absence of substructures in the red pulse to within 2% amplitude modulation.

2. C. E. Max, C. E. McKee, and W. C. Mead, *Phys. Rev. Lett.* **45,** 28 (1980).
3. W. Seka, S. D. Jacobs, J. E. Rizzo, R. Boni, and R. S. Craxton; accepted for publication by *Opt. Comm.*
4. D. J. Kuizenga, *Opt. Comm.* **22,** 156 (1977).
5. A. E. Egorov, V. V. Korobkin, R. V. Serov, *Sov. J. Quant. Electron.,* **5,** 3 (1975).
6. W. H. Lowdermilk, J. E. Murray, D. C. Downs; *LLNL Report* UCRL-50021-74 pp. 2-300-308.
7. G. Albrecht and G. Mourou, submitted to *IEEE J.Q.E.* special issue on lasers for fusion.
8. W. Seka, J. Soures, O. Lewis, J. Bunkenburg, D. Brown, S. Jacobs, G. Mourou, and J. Zimmerman, *Appl. Opt.* **19,** (1980).
9. J. Bunkenburg, W. Seka, J. Soures, submitted to *IEEE J.Q.E.* special issue on lasers for fusion.
10. D. J. Kuizenga, A. E. Siegman, *IEEE J.Q.E.* **6,** 694 (1970).
11. D. J. Kuizenga, D. W. Phillion, T. D. Lund, A. E. Siegman, *Opt. Comm.* **9,** 221 (1973).
12. A. E. Siegman, D. J. Kuizenga, *Opto Electric* **6,** 43 (1974).

1.D GDL Facility Report

The GDL facility continued a high level of operation during the second quarter of FY 81.

A total of 759 shots were delivered by this facility in the period 1 January – 31 March, 1981. The shot distribution was as follows:

3ω Target Experiments	174 Shots
3ω Diagnostics c/o	59
3ω Beam Characterization	42
Damage Test Facility	453
X-Ray Program	31
Total	759 Shots

Details of some of this quarter's work are presented elsewhere in this volume. One of the primary elements of the experimental program on GDL during this time was the 0.35 μm interaction program. Measurements were made of the target absorption with both long (450 psec) and short (100 psec) pulses, the time and spectrally resolved stimulated Brillouin backscatter, x-ray line conversion efficiency, stimulated Raman backscatter, burn through depth (using x-ray spectroscopy), time resolved x-ray emission, x-ray continuum plasma blow-off ion velocity distribution, and beam intensity distribution on target.

Section 2
PROGRESS IN LASER FUSION

2.A High X-Ray Conversion Efficiency with Target Irradiation by a Frequency Tripled Nd:Glass Laser

Recently the high efficiency frequency tripling of a high power Nd:glass laser has been demonstrated.[1,2] The single beam GDL laser system produces pulses of peak power 0.1–0.2 TW at a wavelength of 0.35 μm. Using this laser we measured x-ray production from various plane targets irradiated by short (100 psec) and long (500 psec) UV pulses where the flux on target was varied in the range $10^{13}-10^{15}$ W/cm^2 by changing the beam spot size on target.

The determination of x-ray yield from UV laser-irradiated targets is of interest both in obtaining a signature of the efficiency of coupling laser energy into the target as well as in assessing the target usefulness as an intense x-ray source for probing other samples. Short wavelength lasers ($\lambda < 0.5$ μm) are currently strongly favored as drivers in fusion studies primarily because of their superior coupling to the target.[3] This means higher absorption and a smaller fraction of the absorbed energy which goes into fast electrons. Both of these factors lead to better coupling into the thermal plasma component and should result in a higher intensity of x-rays in the energy range of a few KeV. Indeed we find that for a comparable irradiance on target, tripling the laser frequency leads to about an order of magnitude higher x-ray yield in this photon energy range.

The application of x-rays from a laser target as a probe of *transient* phenomena has recently received increasing attention.

X-ray radiography (back-lighting) is being developed as perhaps the most promising way for diagnosing cold, highly-compressed laser targets.[4] X-rays from laser targets have also been used recently to record the diffraction pattern from a crystal protein[5] and the K-edge fine-structure absorption spectrum of sulfur in a Gypsum crystal.[6] Finally, x-ray pumping leading to lasing in the soft x-ray region has been under active study, employing either resonant or photo-ionization type pumping.[7] In all of these areas the intensity of the x-ray source has been the factor limiting significant progress; the advent of frequency up-converted high power lasers thus opens new possibilities. In some of these applications a quasi-monochromatic source is required (radiography, diffraction, resonant pumping) whereas the others require a wide-band continuum source. We find that both lines and continuum increase significantly in intensity in going from infrared to ultraviolet target irradiation. Furthermore, over the parameter ranges studied, the x-ray intensity was found to depend almost exclusively and nearly linearly on the total laser pulse energy.

The flat targets used in this study (of size 2 × 2 mm and thickness 0.2 mm) were glass, saran, titanium, and nickel. X-ray line spectra

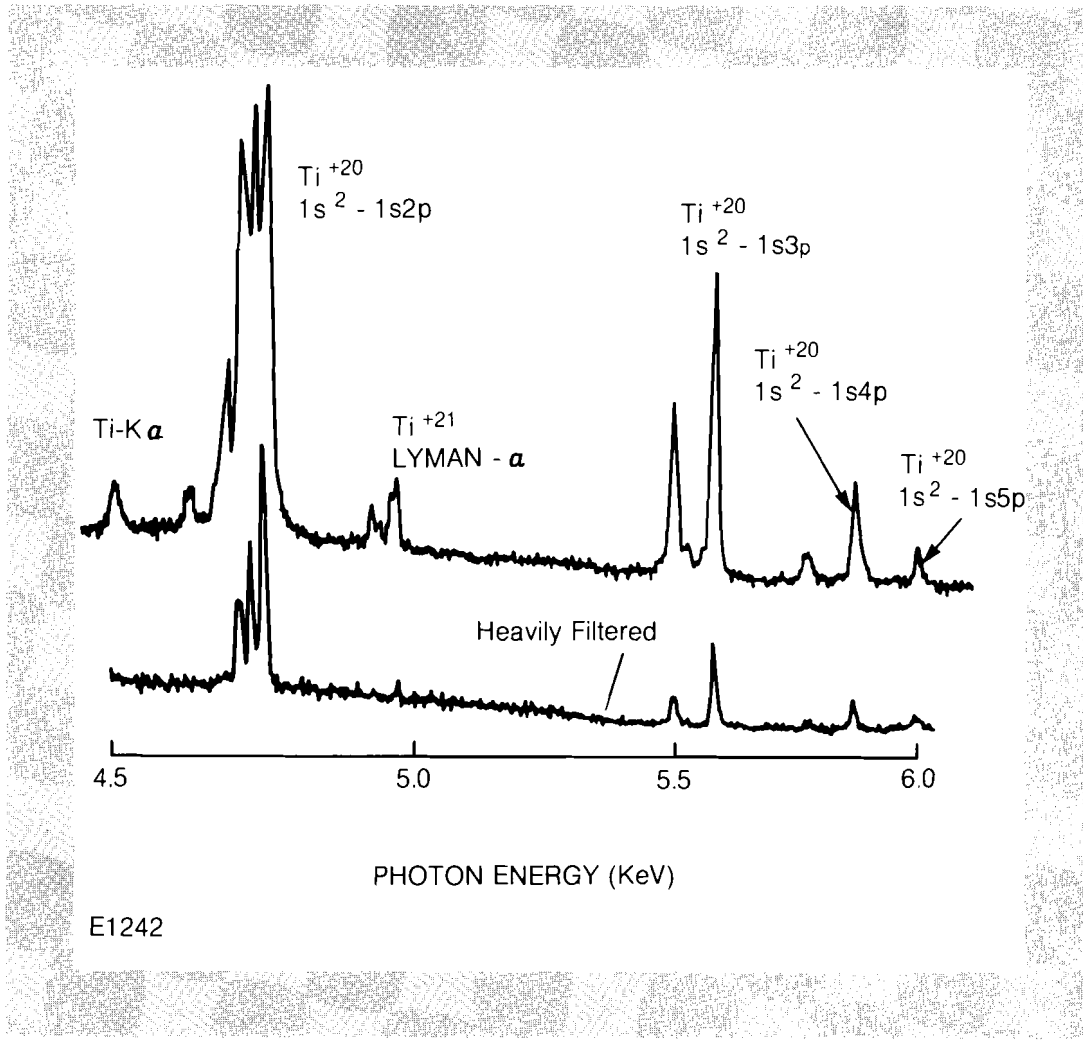

Fig. 11
X-ray spectrum emitted from titanium target irradiated by a 0.35 μm laser (5 × 10¹⁴ W/cm², 500 psec). Lower trace shows the simultaneously obtained spectrum through a 15 μm thick aluminum foil. The filtered spectrum allows the determination of exposure far below the intensity range of film saturation.

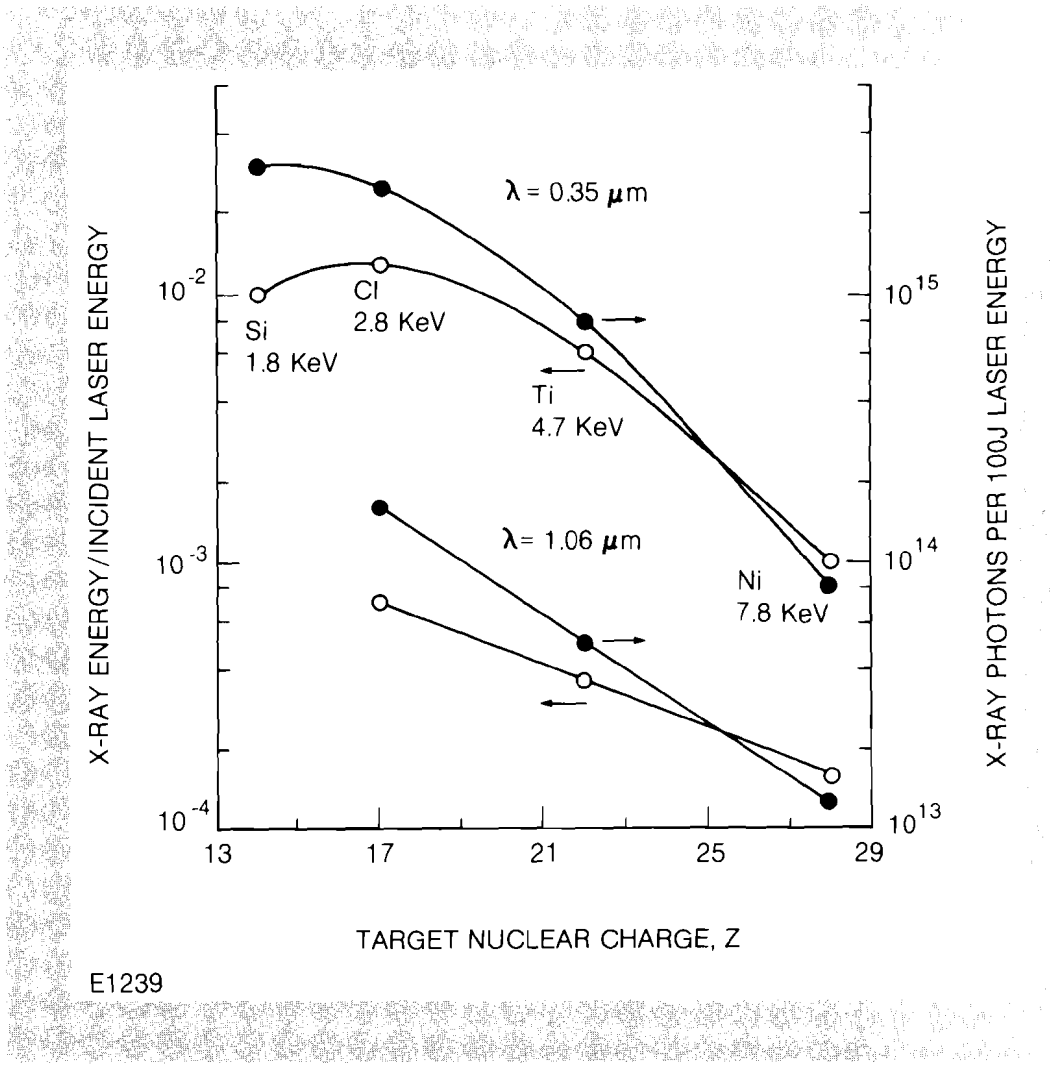

Fig. 12
Quasi-monochromatic x-ray conversion efficiency versus the nuclear charge Z of the emitting ion. X-ray emission into 4π refers to the resonance line $1s^2$-$1s2p$ of the helium-like ionization state including the nearby dielectronic satellite and intercombination lines (Si lines also include the resonance line of the hydrogen-like ionization state). The targets used to obtain these points were: glass, saran, titanium and nickel. The corresponding laser pulse parameters: upper curves: 40 J, 500 psec, 5×10^{14} W/cm²: lower curves: 175 J, 800 psec, 10^{15} W/cm².

of the helium-like and hydrogen-like ionization states of the elements Si, Cl, Ti, and Ni were recorded. Gypsum, P.E.T., germanium, and LiF crystals were used alternatively to record the respective spectra. The diffraction curve and hence the integrated reflectivity of each of them was measured for a set of wavelengths at the National Bureau of Standards. The spectrometer viewed the target at an angle of 45° with respect to the laser beam direction (and the normal to the target). Silicon spectra were recorded on Kodak RAR-2497 film, all other spectra were taken on Kodak No-Screen Medical x-ray film. These films were calibrated using continuous x-ray sources and the results agree well with published data.[8,9].

Figure 11 shows as an example the spectrum obtained from a titanium target irradiated with 40 J, 500 psec pulse focused with an f/12 lens to give an irradiance of about 5×10^{14} W/cm². The lower trace shows the spectrum attenuated by a 15 μm thick aluminum foil, obtained simultaneously. The filtered spectrum allows the determination of exposure far below the intensity range of film saturation. The spectrum consists mostly of lines,

the only significant continuum appearing in the lower-Z Si and Cl spectra beyond the series limit (see below). To obtain quasi-monochromatic radiation a titanium filter can be used; its K-edge is slightly above the $1s^2$-1s2p line thus attenuating strongly the higher energy lines but hardly affecting the intense resonance transition (all elements with $Z > 16$ have this property). We therefore consider the integrated intensity of the resonance line $1s^2$-1s2p of Ti^{+20} along with the adjacent weaker lines, the intercombination lines $1s^2$-1s2p ^3P, and a blend of dielectronic satellites. For Ni these normally weaker lines become more intense than the resonance line. Figure 12 shows the intensity of the comparable transitions of the helium-like ionization state of Si, Cl, Ti, and Ni. For Si we added the intensity of the Lyman-α (1s-2p) line of Si^{+13} which is more intense than the $1s^2$-1s2p line of Si^{+12}, and which cannot be removed using the foil filtration technique described above. The experiments involving glass, saran, and nickel targets had similar irradiation conditions to those of titanium (Fig. 11). The results in Fig. 12 were obtained from the measured intensities by integrating over the full solid angle, assuming spherical symmetry. If the source angular distribution is Lambertian instead, its average intensity will be very close to that at 45° to the surface normal, where the spectrograph was actually located. For the applications listed above one is mostly interested in the intensity per unit solid angle in a given direction. The precision in this quantity is limited by uncertainties in the film calibration curves which we estimate to be within a factor ~ 1.5 based on comparing our calibration with published results.[8,9]

Short laser pulses (100 psec, 0.2 TW) produced nearly the same x-ray conversion efficiency as longer pulses for Si through Ni. Defocusing the laser to lower the irradiance by more than an order of magnitude typically increased the conversion efficiency by a factor < 1.5. All this indicates that x-ray yield scales primarily with total laser pulse energy, at least within the present parameter range. The fact that large focal spots produce more, not less, total emission is favorable for back-lighting where the source angular size has to exceed that of the probed target.

Figure 12 compares these results with x-ray yield data obtained from the same laser operating at 1.054 μm. Its output energy was boosted by four active mirrors[10] to produce 700 psec pulses of 175 J energy. An f/4 focusing lens produced an irradiance of 10^{15} W/cm^2. As seen in Fig. 12, UV irradiation is more efficient in producing x-rays, by a factor of order 10 which decreases with increasing Z. This observation at high Z is believed to be due to the significant presence of fast electrons in IR laser irradiation which can contribute to the excitation of high energy x-ray lines.

In addition to lines, the spectra also display continuum radiation due to recombination; bremsstrahlung radiation is much weaker. As an example we show in Fig. 13 the free-bound continuum due to the recombination process $e^- + Si^{+14} \rightarrow Si^{+13} + h\nu$. The continuum fluence is expressed in terms of KeV/KeV, the

numerator refers to the intensity of the radiation, the denominator to the spectral interval. This unit is numerically equal to the number of photons per energy interval $\Delta E = E$. Again, this fluence is higher by about an order of magnitude than for comparable IR laser irradiation. Integrated over its spectrum ($E > 2.7$ KeV), the total continuum fluence amounts to 2×10^{15} photons, about equal to the number of photons in the $1s^2$ - 1s2p resonance line. Similar intensities of Si continuum have previously been obtained with 100 J pulses of a six beam laser ($\lambda = 1.06\ \mu m$) which symmetrically irradiated and compressed spherical targets.[6] However, continuum intensity comparable to that in Fig. 13 could only be achieved with targets which were optimized for a high density implosion.

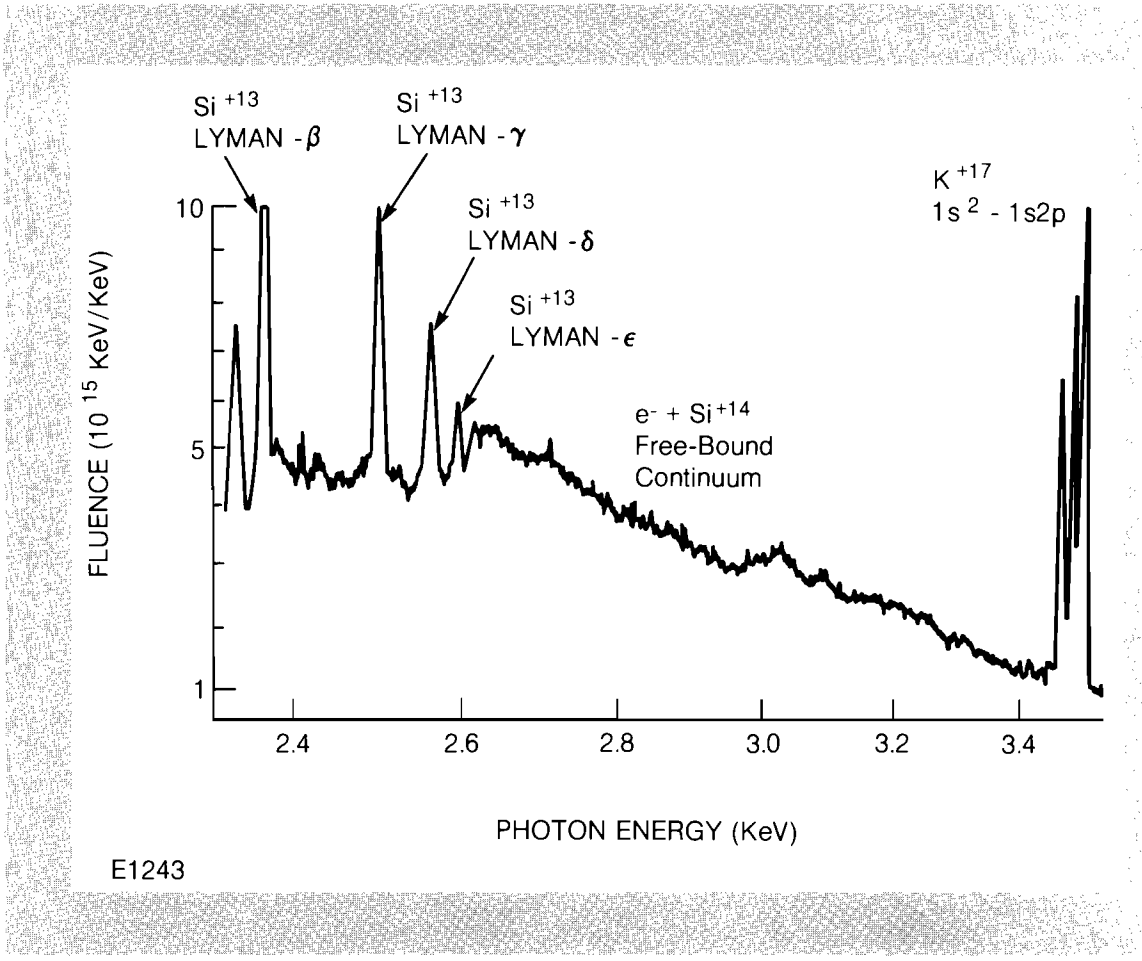

Fig. 13
Free-bound x-ray continuum due to the recombination $e^- + Si^{+14}$ from a glass target irradiated by a 0.35 μm laser (5×10^{14} W/cm², 500 psec). Potassium is an impurity in the glass. The strong potassium and silicon lines extend beyond the figure scale. Silicon radiation is emitted at a lower temperature region ($T \sim 0.7$ KeV) than that of potassium ($T > 1.5$ KeV).

The plasma temperature deduced from the slope of the silicon free-bound continuum is 0.8 KeV. On the other hand, the intensity ratio of the K^{+17} resonance line to the nearby dielectronic satellites[11] yields a temperature of about 2 KeV. This difference, completely in agreement with theoretical predictions of the 1D laser fusion code LILAC, is explained by the temperature profile in the target: lines of higher-Z ions are emitted mostly around peak temperature near the critical layer, whereas lines of lower-Z ions come from inside the critical layer where the temperature is

lower. The fact that lower temperature regions lie further inside the target and have a higher density is the main reason for the decrease in line intensity with increasing Z in Fig. 12.

Figure 14 shows a comparison between measured and calculated silicon continuum (from Fig 13). The calculation was performed with LILAC which includes a radiation transport treatment. The target was represented by a sphere of radius twice as large as the laser focal spot, being subjected to the same irradiance as in the experiment (but a higher total energy). The calculated x-ray intensity was then scaled to the measured laser pulse energy. This procedure is known to give best results when trying to simulate the inherently two-dimensional behavior of flat target irradiation by using a spherically symmetric numerical simulation. The agreement with the experiment is very good, in spite of the estimated uncertainty in the experimental absolute values. Further code runs showed the intensity of the silicon continuum to be

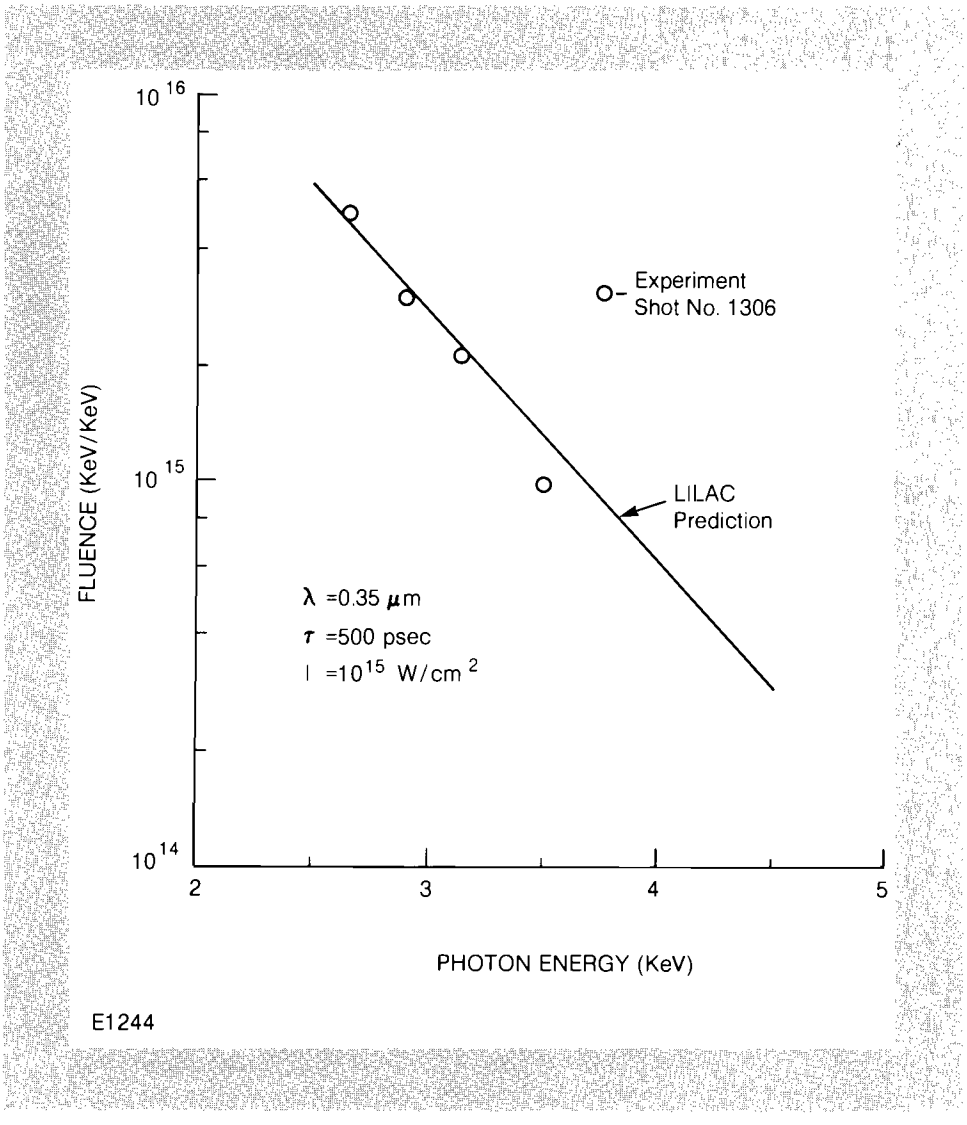

Fig. 14
Comparison of measured continuum spectrum (Fig. 13) with prediction of the one-dimensional laser fusion code LILAC. LILAC includes radiation transport treatment.

very nearly linear in the laser irradiance (for a constant target size) over the range $10^{13} - 10^{15}$ W/cm^2.

A further enhancement of x-ray fluence by an order of magnitude can be expected if UV laser pulses of energy ~ 1 kJ were available and the scaling found here applied at higher intensities. This would mean an irradiance of 10^{14} W/cm^2 or a fluence of 10^{16} photons in either the resonance line of Si^{+12} at 1.85 KeV or the integrated silicon continuum in the range ~ 2.7 – 3.5 KeV, and 2×10^{15} photons (1.5 J) in the 4.7 KeV line of Ti^{+20}. We mention two examples of an application which would be made feasible by such x-ray intensities: (a) the $Si^{+}12$ resonance line at this irradiance would be capable of resonantly pumping[7] the $1s^2$ - 1s 3p transition in Al^{+11} such that gain in the 3-2 transition of Al^{+11} at 4.6 nm may become observable, and (b) for Extended X-ray Absorption Fine-Structure measurements (above an absorption edge)[12] the number of photons above the K-shell edge of, say, Chlorine would be about 10^{10} per resolution element of $\Delta E = 10$ eV at 200 mm from the target, after Bragg diffraction. This would be sufficient to measure EXAFS spectra in systems of dilution down to 100 mM.

REFERENCES

1. W. Seka, S. D. Jacobs, J. E. Rizzo, R. Boni and R. S. Craxton, *Opt. Comm.* **34,** 469 (1980).
2. R. S. Craxton, *Opt. Comm.* **34,** 474 (1980).
3. Annual Report, Ecole Polytechnique, GRECO, 1979; C. E. Max and K. G. Estabrook, University of California, *LLNL Report* UCRL-82671-2 (1979), also Comment on Plasma Physics and Controlled Fusion 5, 239 (1980).
4. M. H. Key, C. L. S. Lewis, J. G. Lunney, A. Moore, T. A. Hall and R. G. Evans, *Phys. Rev. Lett.* **41,** 1467 (1978); C. Bayer, D. Billon, M. Decroisette, D. Juraszek, D. Lambert, J. Launspach, M. Louis-Jacquet, J. L. Rocchiccioli and D. Schirmann, *Laser Interaction and Related Plasma Phenomena* (Plenum Press, New York, 1981) 595; D. T. Attwood, N. M. Ceglio, E. M. Campbell, J. T. Larsen, D. M. Matthews, and S. L. Lane, ibid, 423; C. Yamanaka, S. Nakai, Y. Kato, T. Sasaki, and T. Mochizuki, 541.
5. R. D. Frankel and J. M. Forsyth, *Science* **204,** 622 (1979).
6. B. Yaakobi, H. Deckman, P. Bourke, S. Letzring, and J. M. Soures, *Appl. Phys. Lett.* **37,** 767 (1980).
7. R. W. Waynant and R. C. Elton, *Proc. IEEE* **64,** 1059 (1976); P. Jaegle, G. Jamelot, A. Carillon, and A. Sureau, to be published in *Lasers* (Marcel Dekker, New York, 1981) Vol. 5; A. V. Vinogradov, I. I. Sobelman, and E. A. Yukov, *Sov. J. Quant. Elect.*. **5** 59 (1975); V. A. Bhagavatula, *IEEE J. Q. E.* **QE16,** 603 (1980).
8. R. F. Benjamin, P. B. Lyons, and R. H. Day, *App. Opt.* **16,** 393 (1977).

9. C. M. Dozier, D. B. Brown, L. S. Birks, P. B. Lyons, and R. F. Benjamin, *J. App. Phys.* **47,** 3732 (1976).
10. J. A. Abate, L. Lund, D. Brown, S. Jacobs, S. Refermat, J. Kelly, M. Gavin, J. Waldbillig, and O. Lewis, *App. Opt.* **20,** 351 (1981).
11. C. P. Bhalla, A. H. Gabriel, and L. P. Presnyakov, *Mon. Not. R. Ast. Soc.* **172,** 359 (1975).
12. R. G. Shulman, P. Eisenberger, and B. M. Kincaid, *Ann. Rev. Biophys. Bioeng.* **7,** 559 (1978).

2.B Filamentation of Short Wavelength Laser Beams in Plasmas

A plane electromagnetic beam propagating in a plasma has been shown[1,2,3] to be unstable against modulation in the direction perpendicular to the direction of propagation. This instability causes the beam to break up into narrow filaments of high intensity and low plasma density and is known as the filamentation instability. Such an effect may be important in laser fusion since non-uniformities in illumination at the critical surface may produce non-uniform ablation pressures which will prevent the symmetric implosion of the target. The increased intensity in a filament can drive other plasma instabilities such as stimulated Raman scattering and the two-plasmon instability, these instabilities produce fast electrons which may preheat the fuel.

In a laser produced plasma two mechanisms that can cause the laser beam to form filaments are the ponderomotive force[1] and thermal forces.[4] If the plasma is collisionless the mechanism responsible for filamentation is the ponderomotive force on the electron fluid. This force is proportional to $-\nabla \langle E^2 \rangle / \omega^2$, where E is the electric field of the wave of frequency ω and $\langle\rangle$ denotes time average. The net effect of the ponderomotive force is to push electrons away from regions of highest intensity. However, if the plasma is collisional then inverse bremsstrahlung heating becomes important and filamentation due to thermal effects[4] can occur if the mean free path of an electron, λ_{mfp}, is smaller than the filament width. In regions of higher intensity inverse bremsstrahlung leads to a temperature increase which in turn causes a hydrodynamic expansion. In both cases there results a reduction in plasma density where the intensity is greatest. Since the index of refraction, $N = (1 - 4\pi e^2 n_o / m_e \omega_0^2)^{1/2}$, of a plasma depends on the local electron density, n_o, a decrease in plasma density increases the index of refraction and decreases the phase velocity, $v_p = c/N$, causing the wave fronts to curve in such a way that the beam is focused toward the original region of enhanced intensity becoming even more intense.

As the wavelength of the beam decreases the radiation can penetrate to higher densities where the plasma is more collisional and for a given intensity the ponderomotive force decreases.

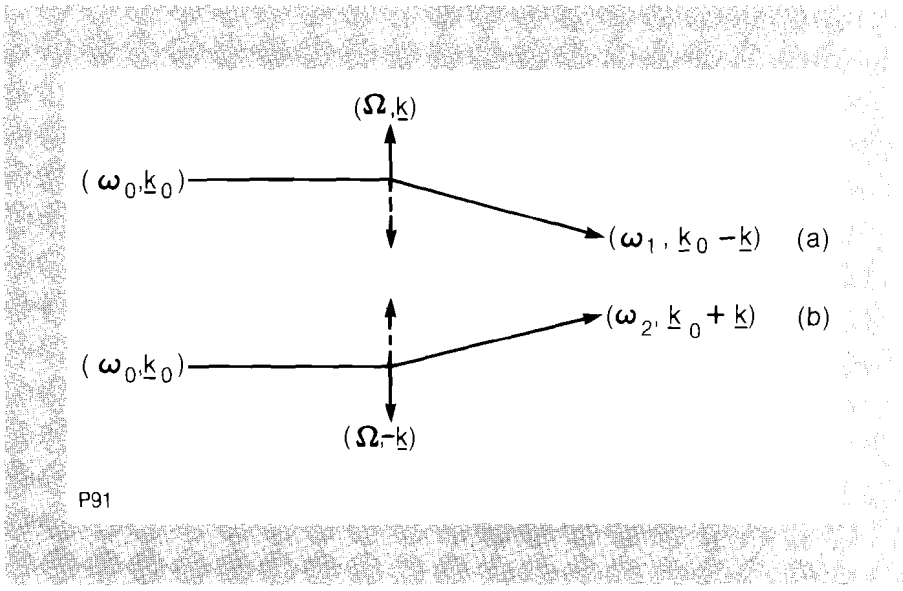

Fig. 15
Configuration of wave vectors for filamentation (a) $(\omega_o, \underline{k}_o)$ the incident electromagnetic wave, $(\omega_1, \underline{k}_o - \underline{k})$ the Stokes electromagnetic wave and $(\Omega, \underline{k})$ a density perturbation; (b) $(w_2, \underline{k}_o + \underline{k})$ the anti-Stokes electromagnetic wave and $(\Omega, -\underline{k})$ a density perturbation. The beating of an incident electromagnetic wave with a density perturbation leads to the generation of Stokes and anti-Stokes electromagnetic waves which grow exponentially if the incident wave intensity is above a threshold value.

Therefore, there will be a regime where both filamentation mechanisms must be considered together.

The filamentation instability is basically a four wave process and is illustrated in Fig. 15. $(\omega_0, \underline{k}_0)$ is the frequency and wavenumber of the initial plane elecromagnetic pump wave which beats with a density perturbation with frequency Ω and wavenumber $\underline{k}$ to produce two sidebands, the Stokes wave with frequency ω_1 $\omega_0 - \Omega$ and wavenumber $\underline{k}_1 = \underline{k}_0 - \underline{k}$ and the anti-Stokes wave with frequency $\omega_2 = \omega_0 + \Omega$ and wavenumber $\underline{k}_2 = \underline{k}_0 + \underline{k}$.

The configuration of the problem is taken to be the following. The initial electromagnetic wave propagates in the x-direction and is polarized in the z-direction and the density perturbation is in the y-direction. The Stokes and anti-Stokes waves are also polarized in the z-direction.

Using a two fluid model together with Maxwell's equations the following equations for the electromagnetic fields and density perturbation can be obtained:

$$c^2\nabla^2\underline{E} - \frac{\partial^2 \underline{E}}{\partial t^2} - \omega_{pe}{}^2\underline{E} = i4\pi e\omega\tilde{n}\underline{v} + 4\pi n_o e\nu_e\underline{v} \quad (1)$$

$$\tilde{n} = in_o e < (\underline{v}\times\underline{B})_y > / k_y k_B T_e - n_o \tilde{T}_e / T_e \quad (2)$$

where c is the velocity of light, ω_{pe} is the plasma frequency, e the charge of a proton, v the electron velocity field due to all the electromagnetic waves, ω the frequency of the electromagnetic field, n_o the equilibrium density, k_y the wavenumber of the density perturbation in the y direction, k_B the Boltzmann constant, T_e the electron temperature, B the magnetic field of the waves, υ_e the electron ion collision frequency and $\tilde{T}_e$ the perturbation of the electron temperature. The first term on the R.H.S. of Eq. (2) represents the ponderomotive force while the second term is due to thermal effects. We have treated the density perturbation as a driven response and neglected ion inertia. Balancing the wave

heating with the thermal conduction term in the energy equation for the electrons and neglecting all other terms allows us to obtain an expression for the electron temperature perturbation T_e in terms of the electromagnetic fields

$$\tilde{T}_e = -eRe < \underline{E}\cdot\underline{v} > /\kappa k_y^2 \quad (3)$$

where Re means real part and κ is the electron thermal conductivity.

We now write the pump, Stokes and anti-Stokes waves as

$$E_j(x,t) = \tfrac{1}{2}\epsilon_j(x,t)\, e^{i(k_j\cdot x-\omega_j t)} + c\cdot c,\ j = 0,1,2$$

where the slow amplitude variation $\epsilon_j(x,t)$ is determined by the non-linear interaction and linear dissipation and the phase factor is due to linear dispersion. Using a perturbation procedure on equations (1)–(3) we obtain the following equations for the Stokes and anti-Stokes waves

$$\begin{aligned}\left(\frac{\partial}{\partial t} + v_1\cdot\frac{\partial}{\partial x} + \gamma_T\right)\epsilon_1(x,t) &= i\Gamma\left(|\epsilon_0|^2\epsilon_1 + \epsilon_0^2\epsilon_2^* e^{-i2\delta t}\right)\\ \left(\frac{\partial}{\partial t} + v_2\cdot\frac{\partial}{\partial x} + \gamma_T\right)\epsilon_2(x,t) &= i\Gamma\left(|\epsilon_0|^2\epsilon_2 + \epsilon_0^2\epsilon_1^* e^{-i2\delta t}\right)\end{aligned} \quad (4)$$

where v_1 and v_2 are the group velocities, γ_T is the damping,

$$\delta = \omega_o - \omega_1,\ \Gamma = \frac{e^2\omega_{pe}^2}{8m_e^2\omega_0^2\omega_1 v_{Te}^2}\left(1 + \frac{1}{2.5k_y^2\lambda_{mfp}^2}\right)$$

and v_{Te} is the electron thermal velocity. The first term in the coupling coefficient comes from the ponderomotive force while the second is due to thermal effects. The ratio between them is a comparison between the strength of the ponderomotive force and thermal force, this ratio is $2.5k_y^2\lambda_{mfp}^2$. Thermal effects can dominate over ponderomotive force effects whenever λ_{mfp} is less than the filament width.

The spatial growth rate in the direction of propagation $k_{||}$ and threshold can be obtained by solving equation (4) for ϵ_0 = constant. The maximum spatial growth rate being given by

$$\left(\frac{k_{||}}{k_0}\right)_{max} = (1/2\,[\,\beta\,(\beta+4c^2/5\omega_0^2\lambda_{mfp}^2)\,]^{1/2} - \gamma_T/\omega_o)/(1-\omega_{pe}^2/\omega_0^2)^{1/2} \quad (5)$$

where

$$\beta = \omega_{pe}^2 v_0^2/4\omega_0^2 v_{Te}^2 \text{ and } v_{0,} = \left|\frac{eE_o}{m_e\omega_o}\right| ,$$

is the quiver velocity in the pump field, maximum growth occurs for $k_y = \omega_o\beta^{1/2}c$. The threshold in terms of v_0 is given by

$$\left(\frac{v_o}{v_{Te}}\right)^2_{threshold} = \frac{8\omega_0^2}{\omega_{pe}^2}\left(\left[(0.4/k_y^2\lambda_{mfp}^2)^2 + (\gamma_T/\omega_0)^2\right]^{1/2} - 0.4/k_y^2\lambda_{mfp}^2\right) \quad (6)$$

Following the treatment of Rosenbluth,[5] Eq. (4) can be modified by the addition of a spatial mismatch, to include the effects of plasma inhomogeneity. We find that the effect of a density gradient on filamentation is just to limit the size of the growth

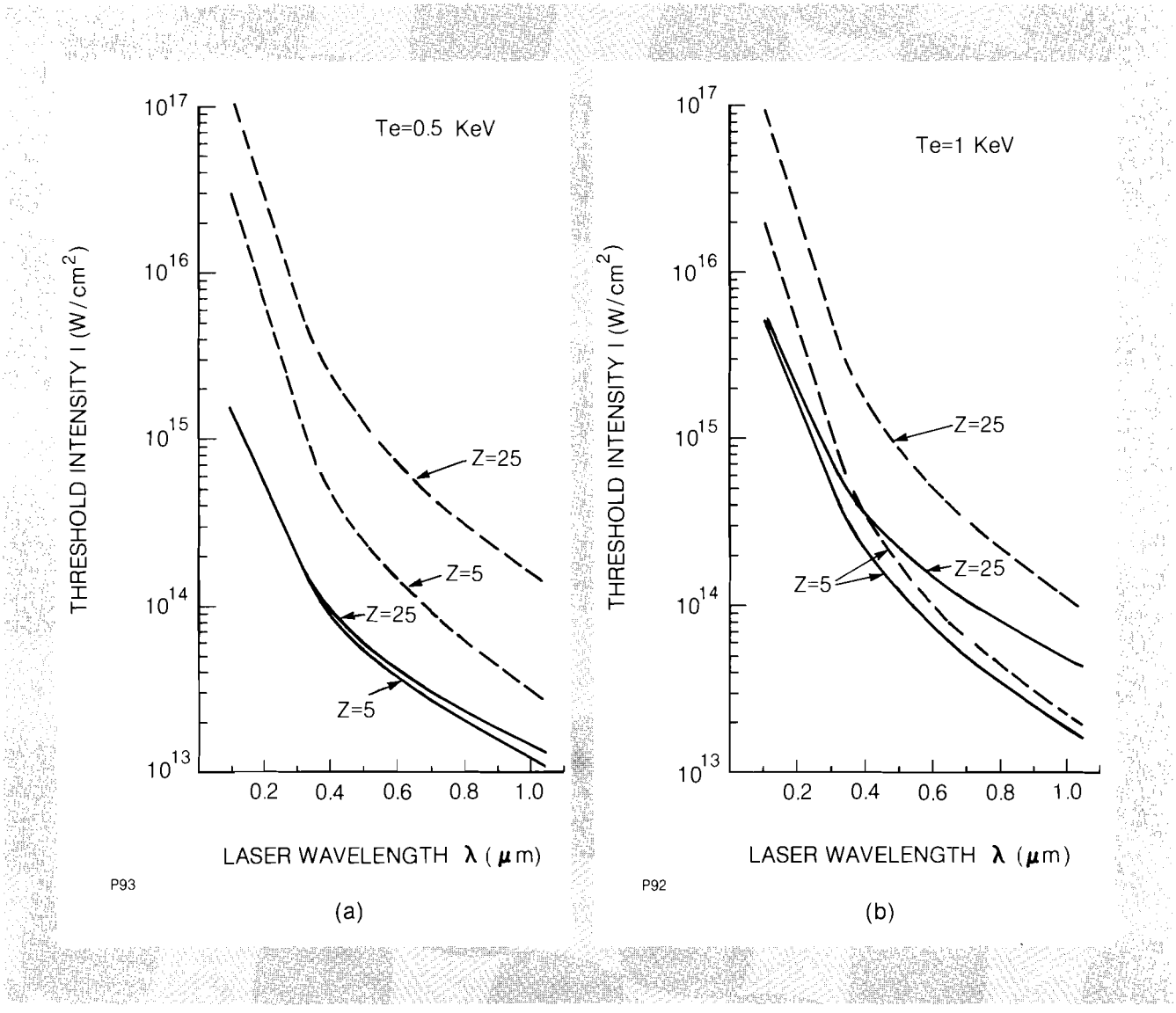

Fig. 16
Laser intensity I(Watts/cm²) for the onset of the filamentation instability as a function of laser wavelength in plasmas at quarter critical with different charge states Z and different temperatures. The solid lines represent the case when both the ponderomotive force and thermal effects are included in the theory. The dashed lines represent the case for the ponderomotive force only.

region. This is in contrast to three wave resonant processes such as stimulated Raman scattering and stimulated Brillouin scattering where a detuning of the resonance occurs. To fully understand the effects of a density gradient on the filamentation instability other effects such as the dependence of the coupling coefficient and damping on x must be taken into account.

The laser threshold intensities for the onset of the filamentation instability as a function of laser wavelength for different charge states Z are plotted in Fig. 16a, 16b. The solid lines represent the case when both the ponderomotive force and thermal effect are included in the equation for the threshold, the dashed lines represent the case when the thermal effect is neglected. For low temperature plasmas the thermal effect is dominant especially for short wavelengths and high Z materials. At higher temperatures, $T_e \sim 1$ KeV, the thermal effect is still dominant at short wavelengths while the ponderomotive force becomes more important at longer wavelengths and low Z materials.

In summary we have shown that for short wavelength lasers and plasma temperatures of about 1 KeV the filamentation mechanism is dominated by the thermal force rather than the ponderomotive force.

REFERENCES

1. P. Kaw, G. Schmidt and T. Wilcox, *Phys. Fluids* **16,** 522 (1973).
2. J. F. Drake, P. Kaw, Y. C. Lee, G. Schmidt, C. S. Lui and M. N. Rosenbluth, *Phys. Fluids* **17,** 778 (1974).
3. R. Bingham and C. N. Lashmore-Davies, *Nucl. Fusion* **16,** 67 (1976).
4. F. W. Perkins and E. J. Valeo, *Phys. Rev. Lett.* **32,** 1236 (1974).
5. M. N. Rosenbluth, *Phys. Rev. Lett.* **29,** 565 (1972).

Section 3

GENERATION OF SUBPICOSECOND PULSES

Fig. 17
Autocorrelation trace of CW Nd:YAG laser. Pulsewidths from 40 - 100 psec are readily obtainable.

We reported results of a synchronously pumped dye laser using a new pumping source in LLE Review Volume 5. A frequency-

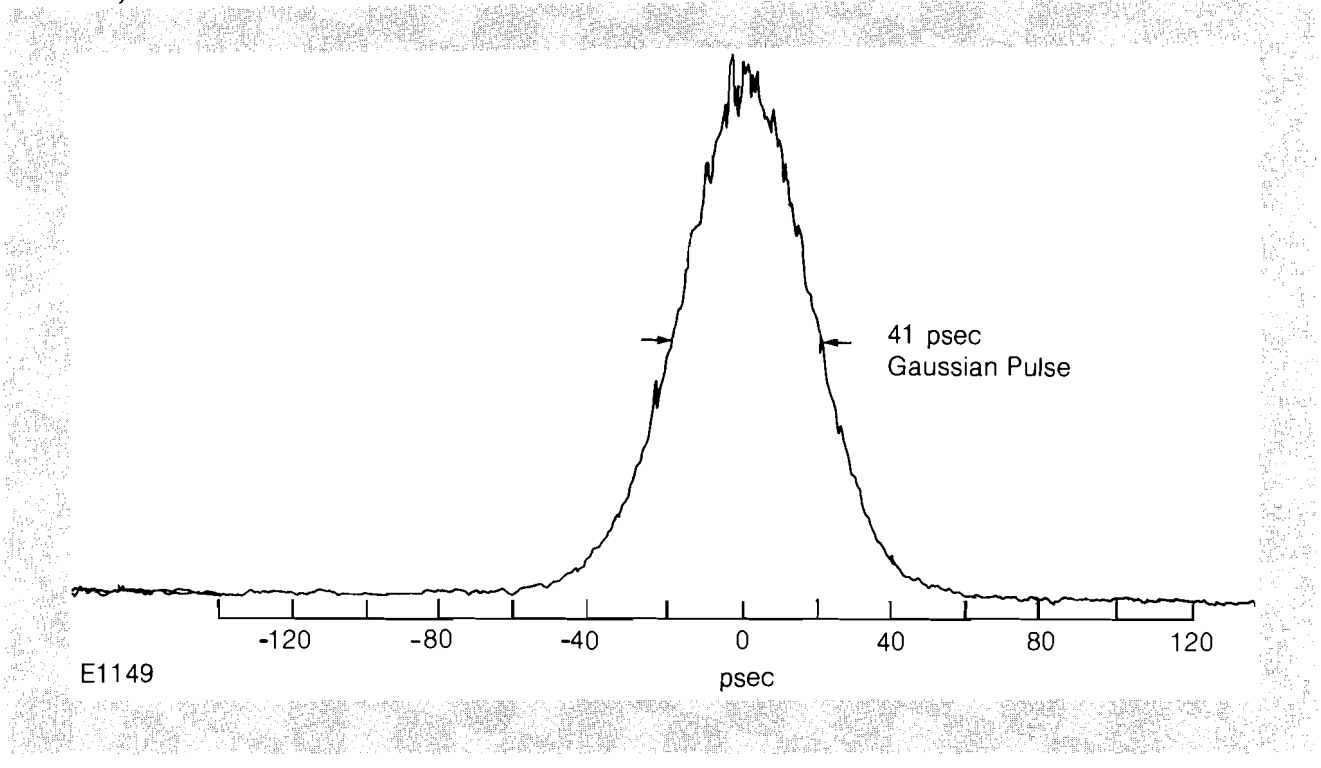

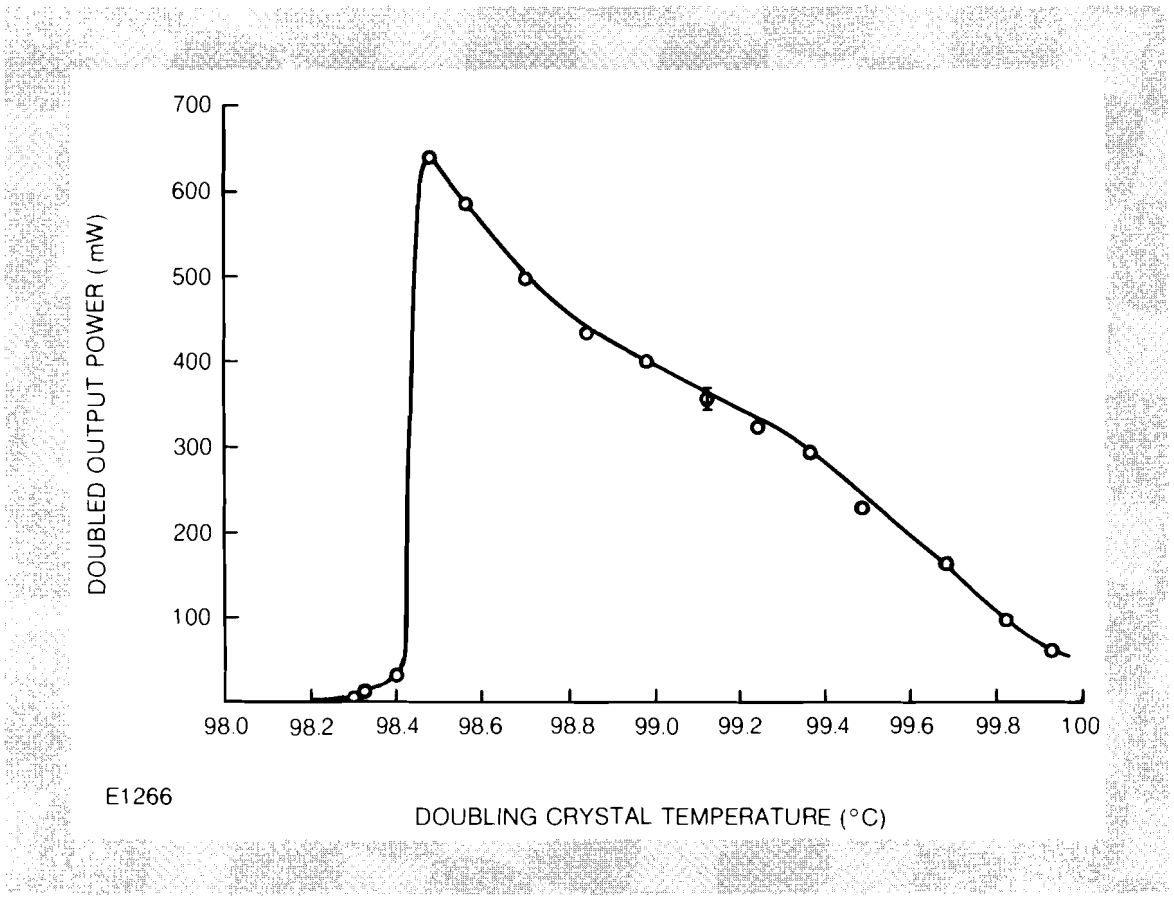

Fig. 18
Conversion efficiency curve for the barium sodium niobate frequency doubling crystal. The peculiar shape of this curve is due to self-absorption of the 0.53 μm frequency doubled output producing localized heating in the doubling region.

doubled neodymium YAG laser is used to pump a rhodamine 6G dye laser. In the previous article we reported pulses as short as 2 psec in an inadequately stabilized experimental setup. Through active and passive techniques we have reduced our sources of instability and produced pulses shorter than 300 fsec.

Many previous authors have reported on the effects of instability and cavity length mismatch on the pulsewidth in synchronously pumped dye lasers.[1,2,3] All of these illuminate the need for a stable pump laser cavity and modelocker and an ultrastable dye laser cavity.

In order to stabilize our Neodymium YAG base we mounted all of the components on a super invar rail. This eliminated any decrease in modelocking efficiency due to typical laboratory temperature variations. A high quality frequency synthesizer (Rockland 6100) was used to drive the acousto-optic (AO) modulator. Careful attention was paid to the correct angle of the AO modulator as it is directly related to the modelocking efficiency and amplitude stability of the Nd:YAG laser. Pulsewidths from 40 psec – 100 psec are obtainable from the Nd:YAG laser shown in Fig. 17.

The barium sodium niobate crystal was temperature stabilized to approximately ± 0.05° C. This variation does, however, produce a significant variation in the output intensity as one must maintain

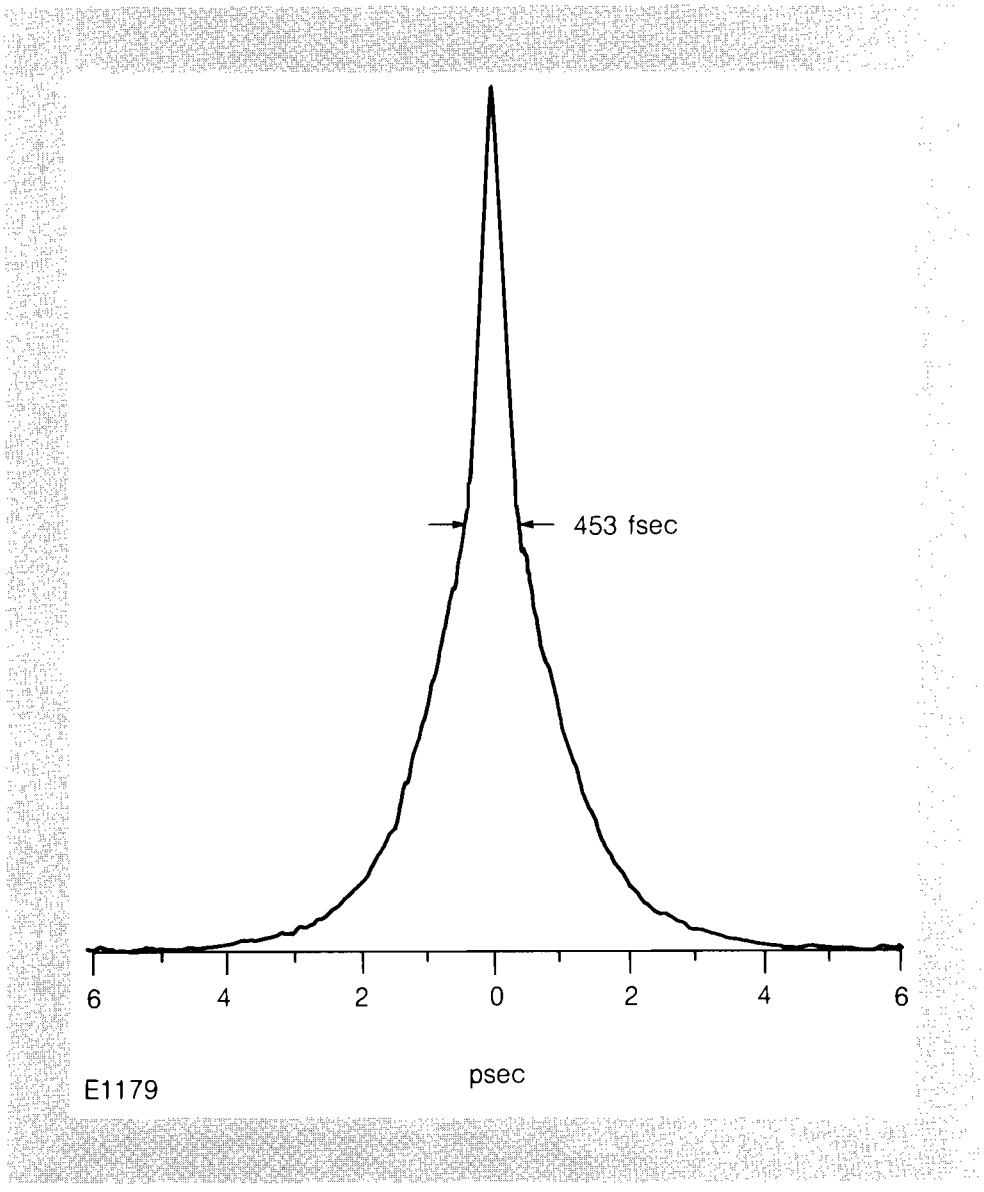

Fig. 19.
Autocorrelation trace of the rhodamine 6G laser. A pulsewidth of 450 fsec is inferred assuming a sech pulse shape.

the temperature on the slope of the efficiency curve of the $Ba_2NaNb_5O_{15}$. Figure 18 illustrates this rather peculiar efficiency curve for the doubling crystal that is due to self absorption of the 0.53 μm frequency doubled output. Absorption of the 0.53 μm radiation produces localized heating in the doubling region requiring one to maintain a lower crystal temperature for optimal efficiency at high powers than at low powers.

The dye laser cavity was also mounted on low thermal expansion super invar. A piezo ceramic crystal is mounted on the end mirror for fine tuning the dye laser cavity. Cavity length fluctuations are primarily a 200 Hz variation of 0.2 μm due to instability in the dye jet. A monomode helium-neon laser was injected into the dye laser cavity and Fabry-Perot fringes were noted as a result of reflections off the two end mirrors. By locking onto one of the fringes and feeding back an error signal to the piezo ceramic

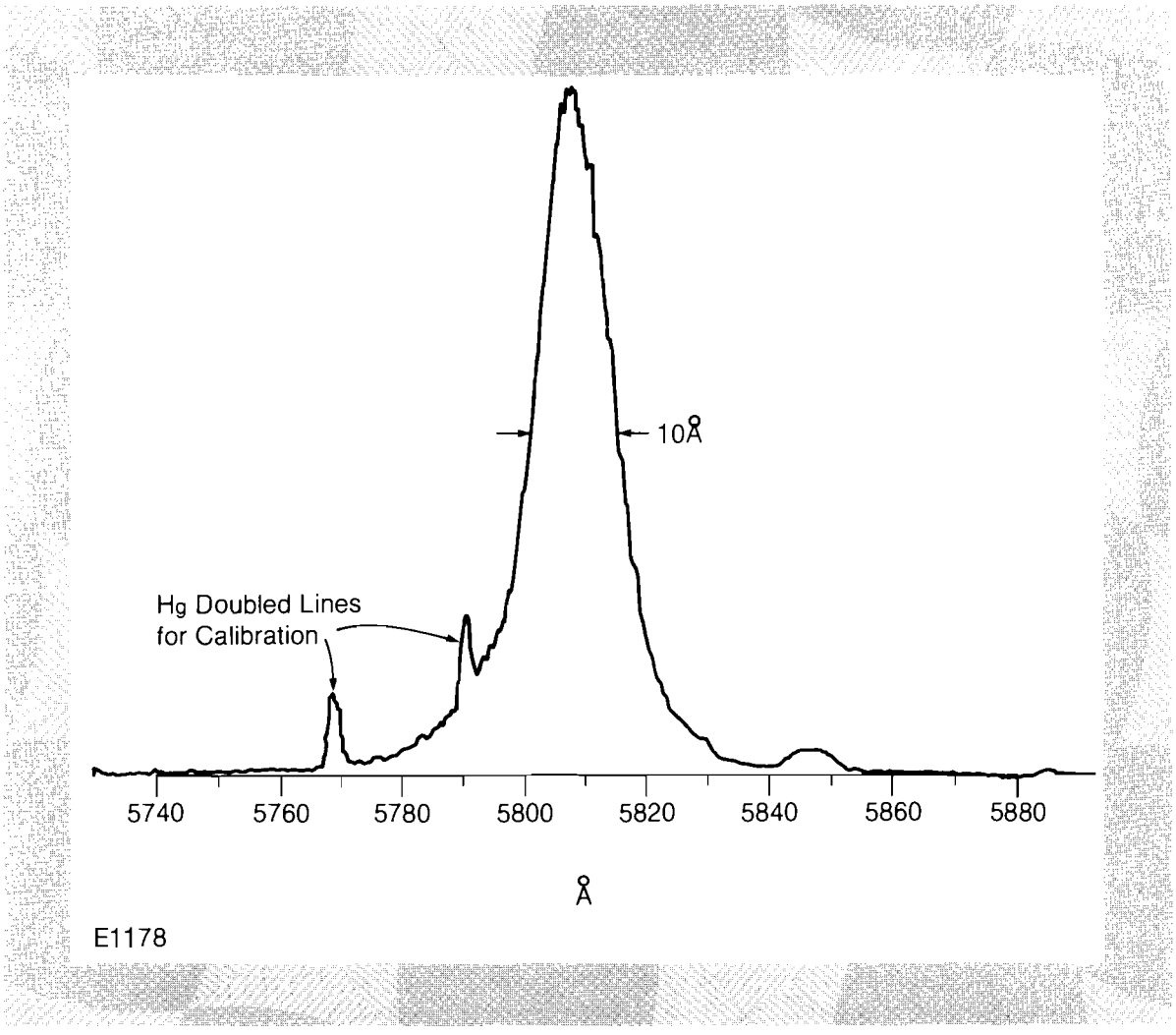

Fig. 20
Spectral output of rhodamine 6G dye laser $\Delta\lambda = 1$ nm. This output together with the pulsewidth of 450 fsec implies that our pulses are nearly Fourier transform limited.

crystal, this cavity length fluctuation was significantly reduced. This feedback did not, however, produce any shorter pulsewidths from the dye laser. As there were no bandwidth limiting elements in the cavity, this negligible improvement in pulsewidth with cavity length stabilization implies that other instabilities in our system are preventing the production of shorter laser pulses.

Through careful matching of the dye laser cavity to the Nd:YAG cavity, pulsewidths of 450 fsec are obtainable as seen in the autocorrelation trace of Fig. 19. The spectral output, as seen in Fig. 20 has a bandwidth of 1 nm indicating a nearly Fourier transform limited pulse. Cavity length detuning results in pulse shapes similar to those in Ref. 4. By adding cresyl violet to our rhodamine 6G to act as a slight saturable absorber, pulsewidths shorter than 300 fsec have been obtained.

REFERENCES

1. Ausschmitt, Jain, and Heritage. *IEEE J. Q. E.* QE-**15,** 912 (1979).
2. A. Scavennec, *Opt. Comm.* **17,** 14 (1976).

3. R. H. Johnson, *IEEE J. Q. E. Elec,* QE-**15,** 840 (1979).
4. Chan, Sari, and Foster, *J. Appl. Phys.* **47,** 1139 (1979).

Section 4

NATIONAL LASER USERS FACILITY NEWS

This report covers the activities of the National Laser Users Facility (NLUF) during the quarter January to March 1981. In this period we have conducted design reviews of equipment to be used on laser experiments, received eight new proposals for the next years, appointed a new NLUF Steering Committee to review proposals, and participated in two scientific meetings to acquaint scientists with the opportunities of research at the NLUF.

The purpose of the design reviews is to guarantee the interface of user equipment on the OMEGA system. The first review finalized the design of a spectrometer for the Physics International experiment (Dr. Glen Dahlbacka). This spectrometer will measure the alpha particles and protons from a DT filled target irradiated by the OMEGA system. The second review was for the University of Illinois (Dr. George Miley). Their review covered the preliminary design of a spectrometer to also measure the alpha and proton reaction product spectra.

The NLUF received eight new proposals during this period, submitted by universities and industries. We now have 15 proposals to be reviewed by the NLUF Steering Committee. The proposals are in the fields of plasma diagnostics, spectroscopy, basic plasma physics, astrophysics, gas breakdown, x-ray diagnostics, physical chemistry, material studies, and laser physics.

The NLUF Steering Committee will meet on April 28. Its purpose is to provide scientific review and merit ranking of proposals and recommend the order of funding for DOE-supported user research funds. Membership of the committee includes scientists from the fields of atomic physics, biophysics, x-ray astrophysics, plasma physics, materials, and laser fusion. A report from the Steering Committee will be available in the next issue of the LLE Review.

The NLUF was represented at two scientific meetings to inform researchers of the opportunities for user experiments at LLE. NLUF was a participant at the invited poster session on national facilities as part of the American Physical Society meeting in Phoenix on March 18. This type of session attracted many useful discussions and interest in potential experiments at NLUF. The facility was also represented at the Third Topical Conference on High Temperature Plasmas in Baton Rouge on February 26.

NLUF now has six ongoing user experiments in various stages of work, from design of diagnostics to experimental data collection.

Further information on NLUF is available from two publications:

i) Experiments with Very High-Power Lasers, The Report of a Workshop,

ii) NLUF Users Handbook, 1981.

These publications can be obtained by writing to:

Dr. Thomas Bristow
Manager, National Laser Users Facility
Laboratory for Laser Energetics
University of Rochester
250 East River Road
Rochester, New York 14623

PUBLICATIONS

Publications

R. Turner and L. Goldman, "Evidence For Multiple Brillouin Modes in Laser-Plasma Backscatter Experiments," *Phys. Fluids* **24,** 184-185 (January 1981).

J. Abate, L. Lund, D. Brown, S. Jacobs, S. Refermat, J. Kelly, M. Gavin, J. Waldbillig, and O. Lewis, 'Active-Mirror: A Large-Aperture, Medium-Repetition Rate, Nd:Glass Amplifier," *Appl. Opt.* **20,** 351-361 (January 1981).

G. Harvey, C. Gabel and G. Mourou, "Synchronization of a Mode-Locked Nd:YAG - Argon Ion Laser System," *Opt. Comm.* **36,** 213-217 (February 1981).

R. McCrory, L. Montierth, R. Morse and C. Verdon, "Nonlinear Evolution of Ablation-Driven Rayleigh-Taylor Instability," *Phys. Rev. Lett.* **46,** 336-339 (February 1981).

J. Rizzo, "Laser Drilling Small Holes for X-Ray Pinhole Cameras," *Rev. of Sci. Instrum.* **52,** 302-303 (February 1981).

T. Dewandre, J. Albritton and E. Williams, "Doppler Shift of Laser Light Reflected From Expanding Plasmas," *Phys. Fluids* **24,** 528-536 (March 1981).

Forthcoming Publications

W. Knox, W. Friedman and G. Mourou, "A Simple Silicon Switch-Driven Psec Streak Camera," accepted for publication by *Applied Physics Letters.*

R. Craxton and R. McCrory, "Two-Dimensional Calculations of Non-Spherical Laser Fusion Implosions," submitted for publication to *Nuclear Fusion.*

S. Skupsky and S. Kacenjar, "Measuring Fuel ρR for Inertial Fusion Experiments Using Neutron Elastic-Scattering Reactions," accepted for publication by the *Journal of Applied Physics.*

M. True, J. Albritton and E. Williams, "Fast Ion Production by Suprathermal Electrons in Laser Fusion Plasmas," accepted for publication by *Physics of Fluids.*

R. McCrory, L. Montierth, R. Morse and C. Verdon, "Taylor Instability in Fusion Targets," to be published in *Laser Interactions and Relative Plasma Phenomena,* Vol. V., Plenum Press.

J. Soures, T. Bristow, H. Deckman, J. Delettrez, A. Entenberg, W. Friedman, J. Forsyth, Y. Gazit, G. Halpern, F. Kalk, R. McCrory, D. Peiffer, J. Rizzo, S. Skupsky, E. Thorsos, B. Yaakobi and T. Yamanaka, "A Review of High Density Laser Driven, Implosion Experiments at the Laboratory for Laser Energetics," to be published in *Laser Interactions and Relative Plasma Phenomena,* Vol. V., Plenum Press.

G. Mourou, C. Stancampiano and D. Blumenthal, "Picosecond Microwave Pulse Generation," submitted for publication to *Applied Physics Letters.*

T. Nordland and W. Knox, "Lifetime of Fluorescence From Light-Harvesting Chlorophyll a/b Proteins: Excitation Intensity Dependence," submitted for publication to *Biophysical Journal.*

J. Kelly, D. Brown, J. Abate and K. Teegarden, "A Dynamic Pumping Model for Amplifier Performance Predictions," submitted for publication to *Applied Optics.*

D. Brown, J. Abate, L. Lund and J. Waldbillig, "Passively Switched Double-Pass Active-Mirror System," submitted for publication to *Applied Optics.*

G. Mourou, "D.C. High Voltage Switching," submitted for publication to *Optics Communications.*

D. Shvarts, J. Delettrez, R. McCrory and C. Verdon, "Self-Consistent Reduction of the Spitzer-Harm Electron Thermal Heat Flux in Steep Temperature Gradients," submitted for publication to *Physical Review Letters.*

S. Kacenjar, L. Goldman and A. Entenberg, "Copper Activation Counter Calibration Using Solid State Track Detectors," accepted for publication by *Review of Scientific Instruments.*

W. Knox and G. Mourou, "A Simple Jitter-Free Picosecond Streak Camera," accepted for publication by *Optics Communications.*

L. Goldman and S. Sarraf, "Effects of Prepulse on Non-Thermal (>10 KeV/Z) Ions in Laser Produced Plasma," submitted for publication to *Physical Review A.*

T. Sizer, G. Mourou and R. Rice, "Picosecond Dye Laser Pulses Using a CW Frequency Doubled Nd:YAG as the Pumping Source," accepted for publication by *Optics Communications.*

S. Sarraf, E. Williams and L. Goldman, "Ion-Ion Two-Stream Instability in Multispecies Streaming Plasma," submitted for publication to *Physical Review Letters.*

This report was prepared as an account of work conducted by the Laboratory for Laser Energetics sponsored in part by the Empire State Electric Energy Research Corporation ('ESEERCO'), Exxon Research and Engineering Company ('EXXON'), the General Electric Company ('GE'), the New York State Energy Research and Development Authority ('NYSERDA'), Northeast Utilities ('NU'), the Standard Oil Company (Ohio) ('SOHIO'), and the University of Rochester ('U of R'). Additional work was sponsored by the U.S. Department of Energy ('DOE') under contract DE-AC08-80DP40124. Neither ESEERCO, EXXON, GE, NYSERDA, NU, SOHIO, DOE, nor the U of R, nor their members or employees, nor any persons acting on their behalf either:

a. Makes any warranty or representation, express or implied with respect to the accuracy, completeness, or usefulness of the information contained in this report, or the use of any information,apparatus, method, or process disclosed in this report may not infringe privately owned rights; or
b. Assume liability with respect to the use of, or for damages resulting from the use of, any information, apparatus, method or process disclosed in this report.

Results reported in the LLE Review should not be taken as necessarily final results as they represent ongoing research.